

INVESTIGATION OF SAND INSTABILITY USING GEOMECHANICS
CRITERIA FOR SANDING PREDICTION

Mr. Kraisingha Meepadung

A Thesis Submitted in Partial Fulfillment of the Requirements
for the Degree of Master of Engineering Program in Petroleum Engineering
Department of Mining and Petroleum Engineering
Faculty of Engineering
Chulalongkorn University
Academic Year 2012
Copyright of Chulalongkorn University

บทคัดย่อและแฟ้มข้อมูลฉบับเต็มของวิทยานิพนธ์ตั้งแต่ปีการศึกษา 2554 ที่ให้บริการในคลังปัญญาจุฬาฯ (CUIR)
เป็นแฟ้มข้อมูลของนิสิตเจ้าของวิทยานิพนธ์ที่ส่งผ่านทางบัณฑิตวิทยาลัย

The abstract and full text of theses from the academic year 2011 in Chulalongkorn University Intellectual Repository (CUIR)
are the thesis authors' files submitted through the Graduate School.

การตรวจสอบความไม่เสถียรภาพของทรายโดยใช้เกณฑ์ทางธรณีกลศาสตร์
เพื่อคาดคะเนการไหลของทราย

นายไกรสิงห์ มีผดุง

วิทยานิพนธ์นี้เป็นส่วนหนึ่งของการศึกษาตามหลักสูตรปริญญาวิศวกรรมศาสตรมหาบัณฑิต
สาขาวิชาวิศวกรรมปิโตรเลียม ภาควิชาวิศวกรรมเหมืองแร่และปิโตรเลียม
คณะวิศวกรรมศาสตร์ จุฬาลงกรณ์มหาวิทยาลัย
ปีการศึกษา 2555
ลิขสิทธิ์ของจุฬาลงกรณ์มหาวิทยาลัย

Thesis Title INVESTIGATION OF SAND INSTABILITY
 USING GEOMECHANICS CRITERIA FOR
 SANDING PREDICTION

By Mr. Kraisingha Meepadung

Field of Study Petroleum Engineering

Thesis Advisor Assistant Professor Sunthorn Pumjan, Ph.D.

Thesis Co-advisor Assistant Professor Suwat Athichanagorn, Ph.D.

Accepted by the Faculty of Engineering, Chulalongkorn University in
Partial Fulfillment of the Requirements for the Master's Degree

.....Dean of the Faculty of Engineering
(Associate Professor Boonsom Lerthirunwong, Dr.Ing.)

THESIS COMMITTEE

.....Chairman
(Associate Professor Sarithdej Pathanasethpong)

.....Thesis Advisor
(Assistant Professor Sunthorn Pumjan, Ph.D.)

.....Thesis Co-advisor
(Assistant Professor Suwat Athichanagorn, Ph.D.)

.....Examiner
(Assistant Professor Jirawat Chewaroungroaj, Ph.D.)

.....External Examiner
(Witsarut Tungsunthomkhan, Ph.D.)

ไกรสิงห์ มีผดุง : การตรวจสอบความไม่เสถียรภาพของทรายโดยใช้เกณฑ์ทางธรณีกลศาสตร์เพื่อ
คาดคะเนการไหลของทราย (INVESTIGATION OF SAND INSTABILITY USING
GEOMECHANICS CRITERIA FOR SANDING PREDICTION) อ. ที่ปริญญาวิทยานิพนธ์
หลัก: ศศ.ดร.สุนทร พุ่มจันทร์, อ.ที่ปริญญาวิทยานิพนธ์ร่วม: ศศ. ดร. สุวัฒน์ อธิษณากร, 85 หน้า.

การผลิตทรายในหลุมผลิตน้ำมันเป็นปัญหาหลักในหลายแหล่งผลิตโดยเฉพาะอย่างยิ่งเมื่อมีการเร่ง
อัตราการผลิตด้วยการเพิ่มอัตราการไหล จึงทำให้เกิดการคลายความแข็งแรงของชั้นหินของแหล่งกักเก็บ
ในขณะที่ทำการผลิต จนทำให้เกิดกระบวนการเคลื่อนตัวของทรายที่เป็นส่วนประกอบในชั้นแหล่งกักเก็บที่
เป็นหินทรายในระหว่างที่มีการไหลของปิโตรเลียมออกมาด้วย

สำหรับกรณีของแหล่งกักเก็บในประเทศไทยโดยเฉพาะแหล่งผลิตน้ำมันดิบบนบกนั้น การศึกษา
ความสัมพันธ์เกี่ยวกับการเคลื่อนตัวของเม็ดทรายในชั้นหินของแหล่งกักเก็บเมื่ออาศัยหลักธรณีกลศาสตร์
เป็นเกณฑ์ และได้ทำการศึกษาวิจัยเพื่อคาดคะเนการการล้มเหลวของทรายโดยยึดตามการประเมินความ
ล้มเหลวของทรายของโมห์คูลอมบี ข้อมูลผลการทดสอบความแข็งแรงของชั้นหินจากห้องปฏิบัติการได้ใช้
ตัวอย่างหิน รวมทั้งข้อมูลการผลิตจากหลุมน้ำมันจากแหล่งน้ำมันดิบบนบกในประเทศไทย ได้ออกแบบการ
วิจัยโดยทำการปรับเปลี่ยนค่าตัวแปรทางธรณีกลศาสตร์ด้วยหลักทางสถิติศาสตร์ประกอบในข้อมูลแรงดัน
และค่าความสามารถในการยอมให้ของเหลวไหลผ่านในแหล่งกักเก็บ ณ สภาวะต่างๆเพื่อสังเกตใน
แบบจำลองของECLIPSE ผลการเปลี่ยนแปลงของแรงดันรอบหลุมผลิตจะใช้วิเคราะห์ตัวบ่งชี้ของการการ
ไหลของทราย

ผลการศึกษาวิจัยพบว่าการเปลี่ยนแปลงตัวแปรแรงยึดตัวในชั้นหินน้ำมันมีผลต่อระดับสูงต่อการ
เสื่อมสลายที่จะเกิดการไหลของทราย ทั้งนี้จากการคำนวณโดยแบบจำลองการเคลื่อนตัวของทรายจะเกิดได้
เมื่อค่าตัวแปรความแข็งแรงยึดตัวได้ถูกกลดลงมาจากค่าเฉลี่ยออกไปสองเท่าของค่าเบี่ยงเบนมาตรฐาน 920
ปอนด์ต่อตารางนิ้ว และจะเกิดขึ้นในทุกกรณีเมื่อเปลี่ยนค่าตัวแปรความแข็งแรงยึดตัวเป็น 343.49 ปอนด์ต่อ
ตารางนิ้ว อย่างไรก็ตามกลับพบว่าตัวแปรทางธรณีกลศาสตร์อื่นๆ อาทิเช่น ค่ามุมเสียดทานภายใน ค่าคง
ตัวปัวซองค์ ค่าคงตัวของยังโมดูลัสกลับไม่มีผลต่อการเสื่อมสลายที่จะเกิดการไหลของทรายแต่อย่างใด
นอกจากนี้ในแบบจำลองพบว่าแรงดันรอบหลุมผลิตจะเปลี่ยนแปลงเมื่อได้รับอิทธิพลจากการเปลี่ยนแปลง
ค่าแรงดันของหลุมผลิต และค่าความสามารถในการยอมให้ของไหลผ่านอย่างมีนัยยะสำคัญ

ภาควิชาวิศวกรรมเหมืองแร่และปิโตรเลียม ลายมือชื่อนิติติ.....
สาขาวิชา.....วิศวกรรมปิโตรเลียม..... ลายมือชื่อ อ.ที่ปริญญาวิทยานิพนธ์หลัก.....
ปีการศึกษา...2555..... ลายมือชื่อ อ.ที่ปริญญาวิทยานิพนธ์ร่วม.....

5271601421: MAJOR PETROLEUM ENGINEERING

KEYWORDS: SANDING / GEOMECHANICS/ SANDSTONE RESERVOIR

KRAISINGHA MEEPADUNG. INVESTIGATION OF SAND INSTABILITY USING GEOMECHANICS CRITERIA FOR SANDING PREDICTION. ADVISOR: ASST. PROF. SUNTHORN PUMJAN, Ph.D., CO-ADVISOR: ASST. PROF. SUWAT ATHICHANAGORN, Ph.D. 85 pp.

Sand production is a major problem in many petroleum fields. Sanding becomes more critical as operators follow more aggressive production strategies. Sand production occurs when the reservoir fluid, under high production rates, dislodges a portion of the formation solids leading to a continuous flux of formation solids into the wellbore; the sanding process may cause complex temporal and spatial changes in permeability in the near-wellbore region.

For Thailand, especially onshore oil field, it is crucial to understand its behaviors of formation as producing sand in view of geomechanic criteria. The study focuses of sand failure by observing the induced stresses near wellbore. The formation failure case adopts the Mohr's Coulomb failure criteria. The rock strength data are collected from the lab test of the onshore field Thailand in addition to its reservoir and production characterization. The variation of rock strength parameters in statistic terms, the reservoir pressure and permeability are tested in ECLIPSE model. Then, the responding induced tresses are observed leading to the indication of sand movement.

As a results of this study show that the sensitivities of cohesion force has significant effect to sand failure. The sand movement is likely to initiate when the cohesion strength reduces to $\mu - stdv$. at 920 psi. And, the confirmed sand movement is clearly stated when the cohesion strength reduces to $\mu - 2 stdv$. at 343.49 psi. While the other rock strength parameter, the internal friction angle, Poisson's ratio, and Young's modulus, have insignificant effect to sand failure. At the same analysis, the reservoir pressure and permeability show impact to induced stresses near wellbore.

Department:Mining and Petroleum Engineering. Student's Signature:.....
Field of Study:...Petroleum Engineering.....Advisor's Signature:.....
Academic Year .2012..... .Co-advisor's Signature.....

ACKNOWLEDGEMENTS

I would like to express my sincere gratitude to my Advisor Asst. Prof. Dr. Sunthorn Pumjan and my co-advisor Asst. Prof. Dr. Suwat Athichanagorn for their guidance and support throughout the thesis. Without valuable comments from them, completion of this work would not have been possible.

I would like to thank my all faculty members in the Department of Mining and Petroleum Engineering who have offered petroleum knowledge, technical advice, and invaluable consultation.

I would like to also thank Schlumberger for providing educational license of ECLIPSE reservoir simulator to the Department of Mining and Petroleum Engineering.

My appreciation goes to my parents for all the care and advice I have received and continue to receive from them. Further thought but not least to thank my wife, Waralak, who always providing a continuous all support, and for our kids for their patience and ultimately love and understanding through my long study.

CONTENTS

	Page
Abstract (in Thai).....	iv
Abstract (in English).....	v
Acknowledgements	vi
Contents.....	vii
List of Tables.....	x
List of Figures.....	xi
List of Abbreviations.....	xiii
Nomenclature.....	xiv
CHAPTER	
I INTRODUCTION.....	1
1.1 Background.....	1
1.1 Outline of Methodology.....	3
1.2 Thesis Outline.....	4
II LITERATURE REVIEW.....	5
2.1 Previous Works.....	5
III THEORY AND CONCEPT.....	9
3.1 Review of Geomechanics Principle.....	9
3.1.1 Geomechanics related parameters.....	11
3.1.1.1 Unconfined compressive strength (USC or Co).....	12
3.1.1.2 Thick wall cylinder strength (TWC).....	12
3.1.1.3 Cohesive strength (So).....	13
3.1.1.4 Internal friction angle (θ).....	13
3.1.1.5 Young's modulus (Es).....	13
3.1.1.6 Poison's ratio (ν_s).....	16
3.1.1.7 Boit poro-elastic factor (α).....	17
3.2 Mohr-Coulomb Failure Criterion.....	18
3.3 Sand Arch Stability and Failure.....	19

CHAPTER	Page
3.4 Sand Failure Criterion.....	20
 IV GEOMECHANIC CRITERIA AND SIMULATION RESERVOIR	
MODEL.....	22
4.1 Geomechanics Test Parameters from Actual data from Onshore Field Data.....	22
4.1.1 Cohesion force.....	22
4.1.2 Internal friction angle.....	23
4.1.3 Poisson’s ratio.....	23
4.1.4 Young’s Modulus.....	24
4.2 Failure Criterion for Study.....	26
4.3 Reservoir Simulation Model.....	26
4.3.1 Grid Selection.....	27
4.3.2 PVT and Fluid Section.....	28
4.3.3 SCAL (Special Core Analysis) Section.....	29
4.3.4 Initialization section.....	31
4.3.5 Schedule section.....	31
4.3.6 Wellbore section.....	32
4.4 Geomechanics input parameters.....	32
 V GEOMECHANIC DETERMINATION AND SIMULATION	
RESULTS AND DISCUSSIONS.....	34
5.1 Base Case Scenario (Case 1).....	35
5.2 Sensitivities of Scenario (Case 2 to Case 17)	38
5.3 Combination of Minimum Rock Mechanics Parameters from Data.....	40
5.4 Calibration of Weakest Rock Mechanics Parameters from Data.....	42
5.5 Effect of Reservoir Pressure	44
5.6 Effect of Reservoir Permeability.....	45
 VI CONCLUSIONS AND RECOMMENDATIONS.....	
6.1 Conclusions.....	48
6.2 Recommendations.....	50

References.....	51
Appendices.....	55
Appendix A.....	56
Appendix B.....	57
Vitae.....	84

LIST OF TABLES

Table		Page
4.1	The Scenario proposed to input in simulation	25
4.2	Grid geometry and properties.....	27
4.3	Geomechanics/Solid.....	28
4.4	Fluid composition of well P-01.....	28
4.5	SWOF: Water/Oil saturation function.....	29
4.6	SGOF: Gas/Oil saturation function.....	30
4.7	Well specification.....	31
4.8	Geomechanics input parameters.....	32
5.1	Base case (case 1).....	34
5.2	Drawdown pressure and oil rate near wellbore (base case).....	36
5.3	Sensitivity cases (2 to 17).....	37
5.4	Case Minimum rock mechanics input parameters.....	40
5.5	Case the weakest rock mechanics input parameters	42
5.6	Observation of well performance under oil rate 200 bpd; K= 20 mD	44
5.7	Observation of well performance comparing K= 20 mD and K =200 mD.....	45

LIST OF FIGURES

Figure	Page
2.1 Arch forming mechanism.....	6
3.1 Rock strength classifications.....	13
3.2 Thick wall core Specimen.....	14
3.3 Stress field figure.....	15
3.4 Stresses in subsurface rock.....	16
3.5 Strain calculation.....	16
3.6 Young's modulus and Poisson's ratio.....	17
3.7 Mohr-Coulomb criterion.....	19
3.8 Illustration of mode of mechanical failure.....	21
4.1 Log Normal Distribution of Poisson's ratio.....	23
4.2 Log Normal Distribution of Young's modulus.....	24
4.3 Water/Oil saturation function.....	29
4.4 Gas/Oil saturation function.....	30
5.1 Grid model of base case from FloViz simulator modeling.....	33
5.2 Zoom in grid near wellbore from FloViz.....	34
5.4 Mohr circle and failure envelope line after case 1.....	36
5.3 Grid coordination reported stresses near wellbore (time step 0.1 days).....	35
5.5 Mohr circle and failure envelope line after case 2 to 5.....	38
5.6 Mohr circle and failure envelope line after case 6 to 17.....	39
5.7 Grid coordination reported stresses near wellbore at time step 0.1 days.....	41
5.8 Mohr's circle and failure envelope line after case Minimum.....	41
5.9 Mohr's circle and failure envelope line after case 2 to 3 against case.....	42
5.10 A grid coordination representing total normal stress and total shear stress as reporting from simulator of case A.....	43
5.11 Mohr's circle and failure envelope line after adopting the weakest rock mechanics input parameters.....	44
5.12 Grid coordination representing total normal stress in X direction from simulator of reservoir pressure 1000, 1800, 2500 Psi.....	45

5.13 Grid coordination reported stresses near wellbore at time step 0.1 days for $K = 200$	46
5.14 Schematic representing case $K = 20$ mD and $K = 200$ mD.....	47

LIST OF ABBREVIATIONS

PI	degree (American Petroleum Institute)
bbl	barrel (bbl/d : barrel per day)
BHP	bottom hole pressure
C ₁	methane
C ₂	ethane
C ₃	propane
i-C ₄ or I-C ₄	isobutane
i-C ₅ or I-C ₅	isopentane
n-C ₄ or N-C ₄	normal butane
n-C ₅ or N-C ₅	normal pentane
C ₆	hexane
C ₇₊	alkane hydrocarbon account from heptanes forward
CO ₂	carbon dioxide
D	darcy
EQUIL	equilibrium data specification
EoS	equation of state
LGR	local grid refinement
M	thousand (1,000 of petroleum unit)
MSCF/D	thousand standard cubic feet per day
PVT	pressure-volume-temperature
PSIA or psia	pounds per square inch absolute
SCAL	special core analysis
STB or stb	stock-tank barrel
STB/D	stock-tank barrels per day
SWAT	water saturation
SWFN	water saturation function
TVD	true vertical depth or total vertical depth

NOMENCLATURE

A	cross-section area
k	permeability
k_r	relative permeability
k_{rg}	gas relative permeability
k_{rw}	water relative permeability
k_{rog}	oil relative permeability for a system with oil, gas and connate water
k_{row}	oil relative permeability for a system with oil and water only
k_{rowg}	oil relative permeability for a system with oil and water at $S_g = 0$
p	pressure
p_c	capillary pressure
q	volumetric flow rate
T	temperature
V	velocity
x	distance
z	compressibility factor
$stdv.$	standard deviation

GREEK LETTER

ε	Corey exponent
ϕ	porosity
α_b	Biot's constant, dimensionless
ε_r	radial strain, dimensionless
ε_{re}	radial elastic strain, dimensionless
ε_z	normal strain in z direction, dimensionless
ε_{ze}	vertical elastic strain, dimensionless
ε_θ	tangential strain, dimensionless
$\varepsilon_{\theta e}$	tangential elastic strain, dimensionless
ν	Poisson's ratio, dimensionless, fraction
σ	total normal stress, m/Lt^2 , psi
σ'	effective stress, m/Lt^2 , psi

ρ	rock density, lb/ft ³
μ	Mean, dimensionless
σ_h	total minimum horizontal stress, m/Lt ² , psi
σ'_h	effective minimum horizontal stress, m/Lt ² , psi
σ'_p	effective radial stress at the interface, m/Lt ² , psi
σ'_r	effective radial stress, m/Lt ² , psi
σ'_v	effective vertical stress, m/Lt ² , psi
σ'_z	effective normal stress in z direction, m/Lt ² , psi
σ'_θ	effective tangential stress, m/Lt ² , psi
τ	shear stress, m/Lt ² , psi
ϕ_f	internal friction angle, dimensionless, degrees

ROMAN LETTER

C_o	Uniaxial Compressive Strength (UCS), m/Lt ² , psi
E	Young modulus, m/Lt ² , psi
G	shear modulus, m/Lt ² , psi
P	average reservoir pressure, m/Lt ² , psi
P_{wf}	bottom hole flowing pressure, m/Lt ² , psi
R_e	radial coordinate, L, ft
R_p	reservoir boundary radius, L, ft = plastic zone radius, L, ft
R_w	cavity radius, L, ft
S_o	cohesive strength, m/Lt ² , psi

CHAPTER I

INTRODUCTION

1.1 Background

Sand production is a major problem in many petroleum fields [1]. Especially in the period of reservoir depletion and increasing of water cut are coincided, thus shortening well life. Sanding becomes more critical as operators follow more aggressive production strategies. Sand production occurs when the reservoir fluid, under high production rates, dislodges a portion of the formation solids leading to a continuous flux of formation solids into the wellbore [2]. As a result, the sanding may compromise oil production, increase completion costs, and erode casing, pipes and pumps, or plug the well if sufficient quantities are produced. Moreover, the sanding process may cause complex temporal and spatial changes in permeability in the near-wellbore region.

For Thailand, especially onshore oil field it is very significant to explore sanding study [3], [4], [5], [6], for unconsolidated sandstone to understand its behaviors. Then, It is also important to be able to predict most likely case, and to provide more aspect of geo-mechanical study relating to sand production prediction performance in such a way that increasing oil production with proper drawdown pressure.

Unfortunately in many case, there is a lack of necessary rock mechanics information for onshore oil field in Thailand to set up a model to study the characteristic of formation failure mechanism.

This thesis aims to understand the interrelationship between rock mechanics parameters and sanding production condition near wellbore based on an available subsurface data and a historical production record from onshore oil field of Thailand. To achieve the prediction of sanding production, review of geomechanical principles

is a key control function to estimate sand production near wellbore. With respect to production historical data and geomechanical information of onshore field in Thailand, it will predict critical drawdown to maximize production with acceptable sand production rate.

In the Northern part of Thailand, there is an onshore concession that has a great amount of oil residing in largely undeveloped reservoirs. One of the problems is severe sand production resulting in shortened well life. This brings the author's attention to study about prediction of sand production from geomechanics point of view. From the investigation of production history and gathering all existing of information from subsurface data, there is a noticeable gap between geomechanics determination and production performance.

In many cases from other research works, the sanding prediction will only be focused on a consolidated sandstone formation. Information obtained from a direct measurement of core samples, log analysis, simulators that predict formation failure and field measurement of solid production are integrated to formulate an empirical equation to predict sanding characterization. Unfortunately direct measurements of core samples are not available in most cases.

This study attempts to find a relationship of changing stress near wellbore against the key rock strength parameters such a cohesion force, the internal friction angle, Young's modulus, and Poisson's ratio.

In this thesis, direct measurement data [4], [5], [6] from the selected wells that has the most complete rock mechanics parameters such as cohesion force, internal friction angle, Poisson's ratio and Young's modulus are analyzed statistically to establish their distribution and their associated statistical parameters. Selection of rock strength input values will follow their statistical inferences within the region of $\mu \mp 2 \text{ stdv}$. In addition to this study the minimum values of rock strength parameters will be used, as defined as the weakest case, in the model. The influence of reservoir pressure and permeability on the sand failure mechanism will also be investigated.

In this study; the failure condition will follow the Mohr's coulomb failure criteria. With the sensitivity of rock strength parameters, production scenario and reservoir pressure, it is anticipated that the mechanical response of sand failure will occur along the variation of these input. And, the proper guideline of critical flow rate can then be determined in light of avoiding sand producing.

1.2 Outline of Methodology

This research aims to study the mechanism of sand failure in a sandstone reservoir with an emphasis on stress behavior analysis around wellbore relating to rock strength properties, reservoir pressure, and permeability variation. Although some research and development have been performed in this area, there still exist many important issues to be simplified and make as a key approach. Specifically, this work focuses on the following aspects:

- Geomechanics determination; rock strength parameters obtained from rock mechanics test are used. Their statistical parameters are quantified. The rock strength values are varied within their statistical limit in most cases of $\mu \mp 2 stdv$.
- As the single reservoir layer, the direct stresses located near wellbore is observed in response to the variation of rock strength, reservoir pressure conditions, and permeability variation as key parameters are varied under sensitivity test.
- Mohr's Coulomb failure criterion is selected to verify the sand movement.

Within this study, the minimum values of raw data cohesion force, internal friction angle, Poisson's ratio and Young's modulus are reviewed from sandstone

core analysis report. Then, these inputs are substituted into a constructed simulation model to create a Mohr's failure envelope line and the corresponding induced stresses.

1.3 Thesis Outline

This thesis paper proceeds as follows.

Chapter II presents a literature review on sand prediction and rock mechanics experiment to investigate sand production behavior, effect to stress around the wellbore and the empirical study associated with sand production study. The chapter includes the advantages and limitations of existing technique of stress prediction for consolidated and unconsolidated formation to improve production performance.

Chapter III describes the theory of rock mechanics input parameters into reservoir model such as cohesion, internal friction angle, Young's Modulus, Poisson's ratio, and their associated laboratory testing.

Chapter IV describes the geomechanics criteria and simulation model used in this study.

Chapter V discusses the results of geomechanics determination of key parameters in reservoir using statistic evaluation and results of simulation obtained from sensitivity test of controlled variables.

Chapter VI provides conclusions and recommendations for further study.

CHAPTER II

LITERATURE REVIEW

This chapter discusses some previous works related to sanding problem in view of rock mechanics parameters relating changing of reservoir pressure and production rate.

2.1 Previous works

In 1957 Hubbert and Willis [8] demonstrated how earth stresses can vary from regions of normal faulting to those thrust faulting. On the basis of a Coulomb failure model, they suggest that the maximum value of the ratio of the maximum to the minimum principal stress in the earth's crust should be about 3:1. They applied an elasticity solution due to Kirsch to solve for the stress around a hole in a biaxial stress field. The effect of fluid pressure in an impermeable hole was superimposed with the above solution using a Lamé' solution for internal pressure in a thick-walled cylinder.

In 1972, Nathan and Hilchie [9] presented a method [20], [27], [28], [30], [34] to estimate critical or maximum production rates possible from friable sandstones without using sand control measures. They estimated formation strength from density and acoustic velocity log data with assuming that the formation face is stabilized if sand arches form around each perforation. Finally estimation of sand production rates from interested intervals will be derived from well test as a critical drawdown pressure is solved.

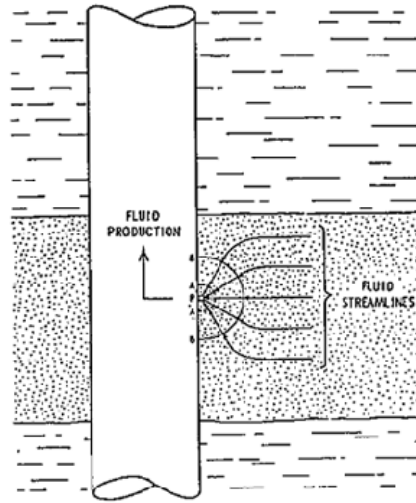


Figure 2.1 Arch forming mechanism

It is observed that critical drawdown will be proportionately greater for stronger formation.

$$(Pr - Pw)_c \propto Es \quad (2.1)$$

Where

Pr is the formation pressure at initial

Pw is the well flowing pressure

$(Pr - Pw)_c$ is critical drawdown pressure

Es is the shear modulus force

Formation of an arch around a single perforation, P , is shown for the case in which production rate is held constant. In a uniform, non-cemented sand formation, the shape will grow spherically and arch BB is formed as perforation is at center of the sphere. The sand is strong enough to resist the fluid-generated force with enough cohesion remaining to stabilize the arch under formation load conditions. Arch AA will be generated smaller in case of some mineral cementation in the formation.

In 1987, K.W. Wiesenberger et al [10] proposed an engineering approach to sand production prediction in 1987 to field in North Sea. Summary of all parameters to represent cavity stability as a function of;

$$\text{Cavity Stability} = f(\Delta P_w, H, \Delta S_h, \Delta S_v, D, F, G, I, L) \quad (2.2)$$

Where

ΔP_w = differential wellbore pressure; “total drawdown” including completion (perforation “skin”) and reservoir drawdown component

H = fluid force factor (incorporates viscosities, relative permeabilities and flow rate)

ΔS_h = net effective horizontal in situ stress

ΔS_v = net effective vertical in situ stress

D = stress-strain deformation parameter from core rock strength testing

F = stress-strain failure parameter from core rock strength testing

G = geometric characteristics of cavities (e.g., perforation length, diameter, and phasing)

I = inclination of borehole and angular relationships between perforation tunnels/cavities and directional (anisotropic) in situ stresses

L = load factor for multiple cycles of flowing and shutting in well

In 1992 Kantzas and Rothenberg [11] and Barrett et al. [12] had determined stress-strain characteristics [31], [32], [33] of sand packs under uniform loads by the use of computer assisted tomography and finite element modeling.

The sanding process is described based on numerical analysis and experimental observations (Nouri et al. [13]). The concepts used in the analysis are evaluated against sanding experiments performed on hollow cylinder samples. The purpose of the experiment was to validate the numerical scheme and study the various parameters that play a role in sanding. The classical Mohr-Coulomb model captured the mechanical response of the porous medium to the applied loading and seepage conditions. The reasonable predictions of the numerical model and their conformity with the experimental observations suggest that the material model and sanding criteria used in the modeling captures the essence of sanding. Examination

of the numerical scheme with field case will provide further confidence in its implementations.

In 2007, J. Zhang et al. [14] used a numerical solution 3D FEMs (Finite Element Methods) to model perforation tunnel stability and sand production under more complicated geometry and stress states. The two cases between an open hole wellbore stability and perforation tunnel stability of gas field in the Northern Adriatic Sea are considered for sand production by simulate critical drawdown under given condition to predict sand arch stability.

In 1981, Risnes et al. [15], [16] studied the near wellbore stress state considering incompressible formation. Steady state fluid flow into the wellbore in a bounded elastoplastic reservoir. For simplicity in this study the pressure in weak drainage area is assumed to be uniform. Bratli and Risnes studied stress state near a sand arch by considering incompressible, steady state fluid flow. Weingarten and Perkins derived an equation describing tensile stresses induced sanding condition in terms of pressure drawdown, wellbore pressure, formation rock cohesion and frictional angle. Dimensionless curves are provided for determining the pressure drawdown at a specific wellbore pressure.

Several sand production prediction methods have been proposed using geomechanical models. These methods could be grouped into analytical (e.g., Risnes et al. [9], Morita et al.[17], Weingarten & Perkins [18], van den Hoek et al. [19]) and numerical models (e.g., Morita et al, [17], Stavropoulou et al. [20], Papamichos & Malmanger [21], Nouri et al. [13]). The analytical models provide formulations for the flow rate required to induce tensile failure. Tensile failure of the material due to seepage drag forces is taken as criterion for sand production.

For onshore Thailand, the focused formation is from LKU-K formation which is at late Miocene age. This formation is widely laid over the central block in Thailand.

CHAPTER III

THEORY AND CONCEPT

This chapter presents the key concepts of the geomechanical determination technique and explanation of dynamic condition with simulator and define related theories involved with the mechanism of Petroleum Geomechanics in an oil reservoir. Previous prospective researches on these issues are also reviewed.

3.1 Review of Geomechanics Principle

Elastic Stress Equations

Steady state rock momentum balance equation in the x, y and z direction can be written as [7];

$$\begin{aligned}\frac{\partial \sigma_x}{\partial x} + \frac{\partial \tau_{yx}}{\partial y} + \frac{\partial \tau_{zx}}{\partial z} &= 0 \\ \frac{\partial \sigma_y}{\partial x} + \frac{\partial \tau_{xy}}{\partial x} + \frac{\partial \tau_{zy}}{\partial z} &= 0 \\ \frac{\partial \sigma_z}{\partial z} + \frac{\partial \tau_{xz}}{\partial x} + \frac{\partial \tau_{yz}}{\partial y} + \rho g &= 0\end{aligned}\tag{3.1}$$

Where ρ is the rock density or a combination of rock and fluid reservoir density, and g is the gravitational constant. The elastic normal stresses σ and shear stress τ can be expressed in terms of strains, ϵ and γ as;

$$\begin{aligned}
\sigma_x &= 2G\varepsilon_x + \lambda(\varepsilon_x + \varepsilon_y + \varepsilon_z) - \alpha P - (2G + 3\lambda)\alpha_T(T - T_r) \\
\sigma_y &= 2G\varepsilon_y + \lambda(\varepsilon_x + \varepsilon_y + \varepsilon_z) - \alpha P - (2G + 3\lambda)\alpha_T(T - T_r) \\
\sigma_z &= 2G\varepsilon_z + \lambda(\varepsilon_x + \varepsilon_y + \varepsilon_z) - \alpha P - (2G + 3\lambda)\alpha_T(T - T_r)
\end{aligned} \tag{3.2}$$

$$\begin{aligned}
\tau_{xy} &= G\gamma_{xy} \\
\tau_{yz} &= G\gamma_{yz} \\
\tau_{zx} &= G\gamma_{zx}
\end{aligned} \tag{3.3}$$

Note that stresses as defined in equation include the pore pressure and Biot constant and are, therefore, total stresses. Constant G , also known as the shear modulus, and λ are Lamé's constants. They are function of Young's modulus, E , and Poisson's ratio, ν ;

$$G = \frac{E}{2(1+\nu)}, \quad \lambda = \frac{E\nu}{(1-2\nu)(1+\nu)}, \tag{3.4}$$

Strains $\varepsilon_{x,y,z}$ are defined in terms of displacements in the x,y,z directions, namely u , v and w thus;

$$\begin{aligned}
\varepsilon_x &= \frac{\partial u}{\partial x} & \varepsilon_y &= \frac{\partial v}{\partial y} & \varepsilon_z &= \frac{\partial w}{\partial z} \\
\gamma_{xy} &= \frac{\partial u}{\partial y} + \frac{\partial v}{\partial x} & \gamma_{yz} &= \frac{\partial v}{\partial z} + \frac{\partial w}{\partial y} & \gamma_{zx} &= \frac{\partial w}{\partial x} + \frac{\partial u}{\partial z}
\end{aligned} \tag{3.5}$$

According to Hibbitt et. al [22], ABACUS Theory Manual was mentioned and total stress can be calculated as follow;

$$\sigma_T = \sigma_{\text{eff}} - \alpha P \tag{3.6}$$

Where σ_T is the total stress, σ_{eff} is the rock effective stress, α is Biot's constant and P is the pore (fluid) pressure. Note that in Geomechanics we normally defined convention sign of tensile stresses as positive, and compressive as negative.

This similarity of elastic stress equations are also applied in simulation model in this study.

3.1.1 Geomechanics related parameters

To obtain geomechanics properties, it is necessary to have a test core sample and observe its failure characteristic in the laboratory. This kind of test is measured the direct response of core sample as the simulated external pressure is applied. The most represented result is a Triaxial load test (TXL). This test is carried out to identify the principle stresses by varying a confining pressure applied to core samples. [35], [36], [37].

Rock strength parameters derived from rock mechanics core test are;

- Unconfined compressive strength (UCS or C_0)
- Thick wall cylinder strength (TWC)
- Cohesive strength (τ_0)
- Friction angle (θ)
- Young's modulus (E)
- Poison's Ratio (ν)
- Boit Effective stress coefficient (α)

Theoretically we can only obtain direct and definitive data where they are only available from rock mechanics test on core. It is rare to get all information from the fact that core is discontinuous and rock strength data coverage is inherently limited by core itself. In this case, the log indicators information will be used to calibrated against the available core data.

3.1.1.1 Unconfined Compressive Strength (UCS or Co)

UCS is the minimum stress that rock start to break apart or the maximum stress that rock is not deformed when no pressure is applied to pore space. It is measured in stress or pressure unit such as psi, or MPa.

Figure 3.1 shows range of UCS for any rock strength. UCS can be measured either by direct measurement from lab experiment or deriving from log data.

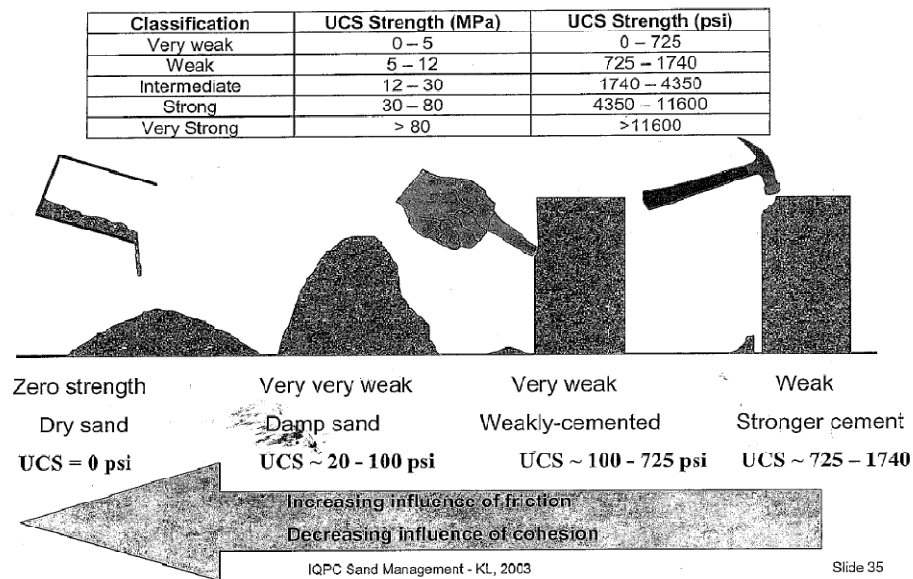


Figure 3.1 Rock strength classifications.

3.1.1.2 Thick Wall Cylinder (TWC)

This parameter is strength of specific condition which attempt to mimic perforation tunnel or wellbore. Core is cut to cylinder shape, as seen in Figure 3.2. Stress is applied from outside cylinder until the specimen is collapsed. TWC is measured in unit of stress or pressure such as psi.

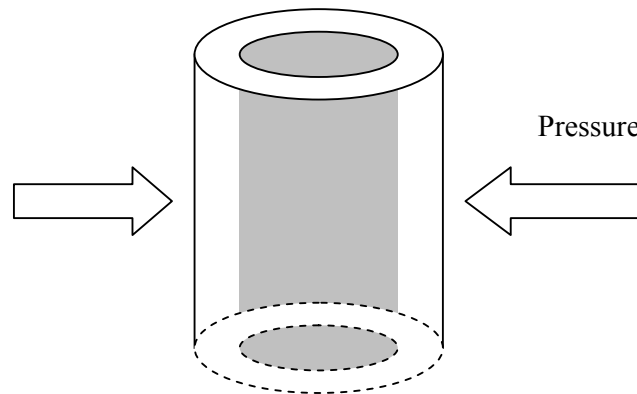


Figure 3.2 Thick Wall Core Specimen.

3.1.1.3 Cohesive strength (S_o)

Cohesive strength is force that act as cementation of solid grains in the formation. The cohesive strength is derived from the multiple Triaxial load test.

3.1.1.4 Internal Friction angle (θ)

Friction angle is the angle acting between each grains resulting to shear force. The internal friction angle is derived from the multiple Triaxial load test.

3.1.1.5 Young's Modulus (E)

Young's modulus or elastic modulus is a tendency of the object to be deformed in the direction perpendicular to the surface after subject to force. It can be described in the term of slope in elastic zone of the stress and strain curve, as seen Figure 3.. Elastic zone is the regions that object can reform to original shape after deformed by external force whereas in plastic zone, object cannot resume the initial state. Young's modulus can be expressed as mathematical equation as follows.

$$E = \frac{\text{Stress}}{\text{Strain}} = \frac{\sigma}{\varepsilon} \quad (3.7)$$

Where:

Stress (σ) is internal force per area which balances or counteracts external forces.

It can be described as tensors with nine components. Three normal stresses (σ) are acting perpendicularly to considering surfaces while six shear stresses (τ) are parallel to the surfaces subjected to force, please as seen in Figure 3.3.

Solid, liquid, and gases have stress fields. At static condition, hydrostatic pressure is equivalent to fluid normal stress whereas shear stress forces fluid to move.

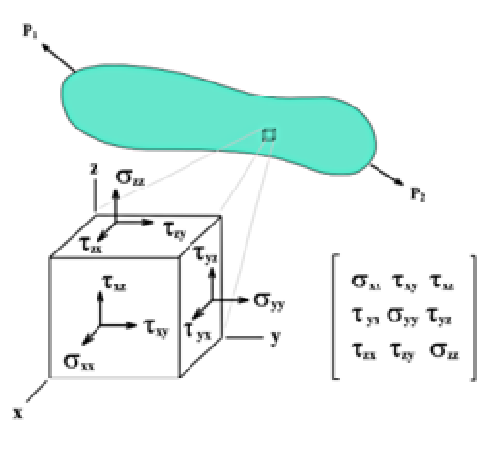


Figure 3.3 Stress field [4]

Three main principles (normal) stresses can be directly calculated from field data, as seen in Figure 3.4. Firstly, vertical stress (σ_v) is an overburden pressure or in the other words it is weight of formation above the considering position. This principle stress can be easily estimated using global correlation or log derived formation density. Secondly, the minimum horizontal stress is normally the smallest stress acts on rock. It can be calculated using LOT or FIT test data as the fracturing pressure is equivalent to the minimum stress. Thirdly, the maximum horizontal stress is normally the middle in magnitude among the principle stresses.

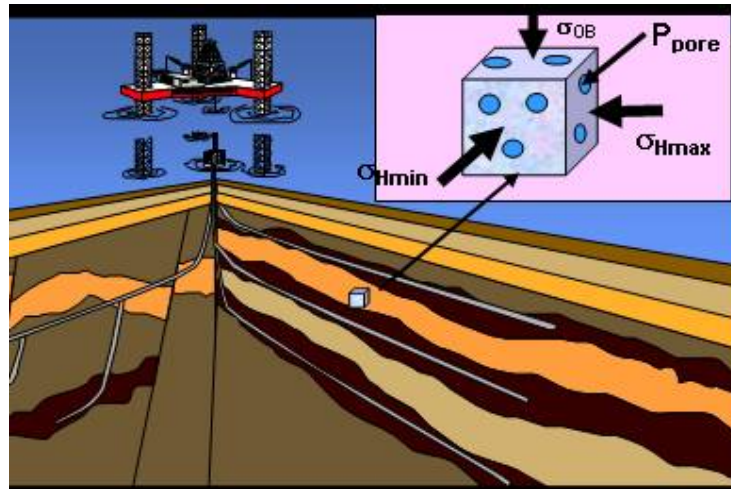


Figure 3.4 Stresses in subsurface rock.[4]

Strain (ϵ) is the geometrical expression of deformation caused by the action of stress on a physical body. Strain is calculated by first assuming a change between two body states: the beginning state and the final state. Then the difference in placement of two points in this body in those two states expresses the numerical value of strain. Strain therefore expresses itself as a change in size and/or shape”, courtesy Wikipedia website, as seen in Figure 3.5.

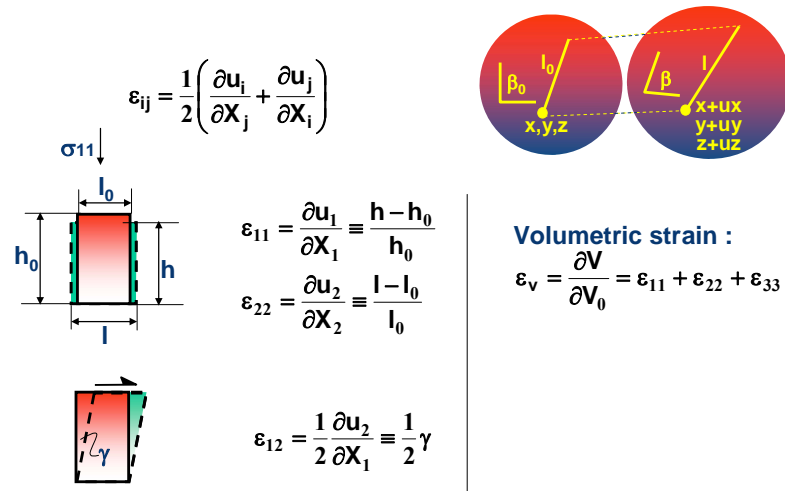


Figure 3.5 Strain calculation.

3.1.1.6 Poisson's Ratio (ν)

When object subjects to external force, it tends to thinner in the same direction with force whereas thicker in the direction perpendicular to the force. Poisson's ratio is the ratio of radial strain to axial strain. Poisson's ratio can be expressed as mathematical equation as shown in Figure 3..

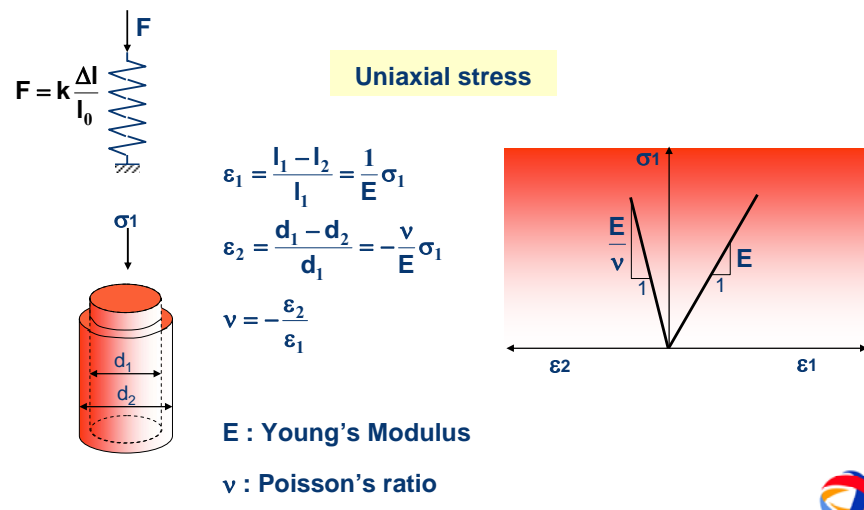


Figure 3.6 Young's modulus and Poisson's ratio.

3.1.1.7 Biot's Effective stress coefficient (α)

The Biot's effective stress coefficient of rock is an important poro-elastic parameter that relates stresses and pore pressure. It describes how change in pore pressure affects rock stress. The difference is due primarily to different compressibility between rock material and fluid in pore space. Biot's coefficient is in the range of 0.0-1.0 and also called pro-elastic factor. The parameter is mathematically expressed as follows.

$$\alpha = 1 - \frac{C_r}{C_{bc}} \quad (3.8)$$

Where:

C_r is rock grain compressibility and

C_{bc} is rock bulk compressibility.

For sonic logging and waveform analysis, it will indirectly provide a means for obtaining an estimate of mechanical properties of the in-situ rock. The following rock properties can be obtained from suitable log data:

$$\text{Poisson's Ratio, } \nu = \frac{\frac{1}{2}(\Delta t_s / \Delta t_c)^2 - 1}{(\Delta t_s / \Delta t_c)^2 - 1} \quad (3.9)$$

$$\text{Shear Modulus, } G = 1.34 \times 10^{10} \frac{\rho_b}{\Delta t_s^2} \quad (3.10)$$

$$\text{Young's Modulus, } E = 2G(1 + \nu) \quad (3.11)$$

$$\text{Bulk Modulus, } K_b = 1.34 \times 10^{10} \rho_b \left(\frac{1}{\Delta t_c^2} - \frac{4}{3\Delta t_s^2} \right) \quad (3.12)$$

$$\text{Bulk Compressibility, } C_{bc} = \frac{1}{K_b} \quad (3.13)$$

where:

Δt_c = compressional wave travel time, $\mu\text{secs/ft}$

Δt_s = shear wave travel time, $\mu\text{secs/ft}$

ρ_b = bulk density, g/cc

1.34×10^{10} = conversion factor, applicable to these units.

3.2 Mohr-Coulomb Failure Criterion

This criterion [7] relates the shearing resistance to the contact forces and friction, to the physical bonds that exist among the rock grains [Jaeger and Cook, 1979]. A linear approximation of this criterion is given by:

$$\tau = \tau_o + \sigma \tan \phi \quad (3.14)$$

For a producing well, it is assumed that σ_o is the maximum principle stress and σ_r is the minimum principle stress. The failure envelop line touches Mohr Circle as shown in Figure 3.1

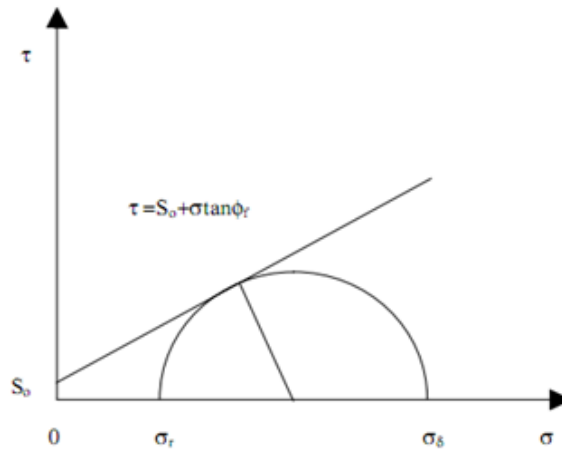


Figure 3.7 Mohr-Coulomb criterion. [7]

Relationship between maximum principle stress and the minimum principle stress can be derived in terms of;

$$\frac{\sigma'_\theta - \sigma'_r}{2} = \frac{\sigma'_\theta + \sigma'_r}{2} \sin \phi_f + S_o \cos \phi_f \quad (3.15)$$

By rearranging, yield

$$\sigma'_r - \sigma'_\theta = -\frac{2 \sin \phi_f}{1 - \sin \phi_f} (\sigma'_r + S_o \cot \phi_f) \quad (3.16)$$

3.3 Sand Arch Stability and failure

After Zhang J. et. al [14], The arch serves to support a load by resolving the vertical stress into horizontal stress. When the arch fails, the sand production begins. Assuming an idealized production cavity and full spherical symmetry of the stress field, the following sand arch stability criterion was derived.

$$\frac{\mu q}{2\pi k r} < 2 UCS \quad (3.18)$$

Where:

UCS is the uniaxial/unconfined compressive strength of the formation

q is the flow rate of the cavity

k is the formation permeability

r is the cavity radius and μ is the fluid viscosity

As fluid flow is introduced, the effect of the drag forces is to increase the depth of the failed zone. R. Risnes et al (SPE12948) derived a fundamental stability criterion as

$$\frac{\mu q}{2\pi k r} = \frac{T+1}{T} \cdot 4 \tau_o \cdot \tan \alpha \quad (3.19)$$

Where:

μ is fluid viscosity

q is fluid flow rate per arch

Kc is permeability in the partly failed zone

r is arch (cavity) radius

α is failure angle of the sand

τ_o is cohesive strength of the material in the the partly failed zone

T is $2(\tan^2 \alpha - 1)$

The arch serves to support a load by resolving the vertical stress into horizontal stress. When the arch fails, the sand production begins, assuming an idealized production

3.4 Sand Failure Criterion

Next, the correlation for study well is developed in this thesis. However to make it simple for evaluation, the input parameters are setup in the simulator to observe the effects of changing drawdown pressure and flowing bottom hole pressure. The stress near wellbore will be observed. According to Amos S. Kim et. al [26] and Tippie, D.B., and Kohlhass, C.A [23] and Burton R. et. al [24] and Qiu et. al [24] and Dake L.P.[33], sand failure criterion is introduced due to sand failure and erosion model.

It is also confirmed from van den Hoek [19] that initial failure is driven by external stresses rather than drawdown. However Nathan Stein and D.W. Hilchie [9] assume the critical drawdown will be proportionately greater for stronger formation or;

$$(P_R - P_w) \alpha E_s \quad (3.20)$$

Where:

P_R is reservoir pressure

P_w is well flowing pressure

E_s is shear modulus

These statements support assumption in this paper to monitor the state of stresses near wellbore against different well production scenarios.

In conclusion, sanding will occur under risk of perforation collapse from 1) tensile 2) shear failure, and 3) combination of drawdown and depletion, which need to be observed during operational well life as shown in Figure 3.8

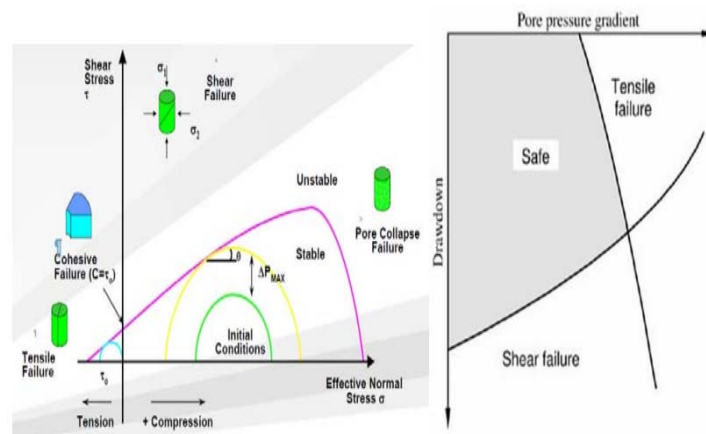


Figure 3.8 Illustration of mode of mechanical failure after *Amos S. Kim et. al* [25]

CHAPTER IV

GEOMECHANIC CRITERIA AND SIMULATION RESERVOIR MODEL

In order to represent the geomechanic characterization of the studied reservoir and its effect on the original stress near wellbore, we used ECLIPSE E300 simulation program (compositional simulator). This simulation program is only tool to report a calculation of stresses as varying rock strength from the direct core testing data such as cohesion force, internal friction angle, Poisson's ratio, and Young's modulus. The principle of Mohr-coulomb failure criteria is applied as a failure condition as the moving sand initiate.

4.1 Geomechanics Test Parameters from Actual Data from Onshore Field Data

The key parameters for sand failure condition in the formation are brought from actual data from onshore case, Thailand [3]. This study cover full test of 42 core samples of sandstone formation. All data are used to find the most representative statistics. The plot of distribution model for key parameters and their associated statistical inference are shown as follows.

4.1.1 Cohesion force

There are 11 data samples representing as sandstone from total 42 core samples of collecting from the multiple Triaxial tests on sandstone core specimen. The best cohesion data are best fit by Beta General distribution with mean and standard deviation (stdv.) of 1497.31 psi and 576.91 respectively.

4.1.2 Internal friction angle

There are 11 data collecting from the multiple Triaxial test on sandstone core specimen. The internal friction angle data are best fit by Beta General distribution with mean and standard deviation (stdv.) of 29.87 degree and 6.64, respectively.

4.1.3 Poisson's ratio

The total of 64 Poisson's ratio values obtained from the lab test are plotted using software @RISK as shown in Figure 4.1. The Poisson's ratio data are best fit with log normal distribution model with mean and standard deviation of 0.28 and 0.068, respectively.

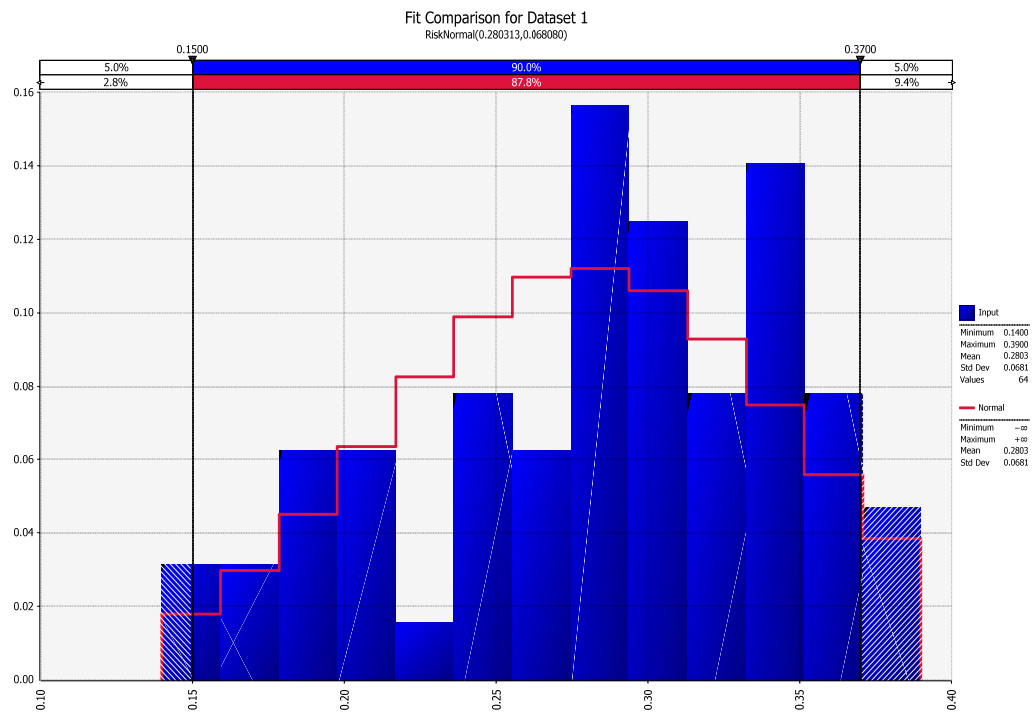


Figure 4.1 Log Normal Distribution of Poisson's ratio. [3]

4.1.4 Young's Modulus

The total of 71 Young's modulus values obtained from the lab test are plotted using software @RISK as shown in Figure 4.2. The Young's modulus data are best fit with log normal distribution model with mean and standard deviation of 10.19 GPa (1,477,550 Psi) and 4.98 GPa (722,100 Psi), respectively.

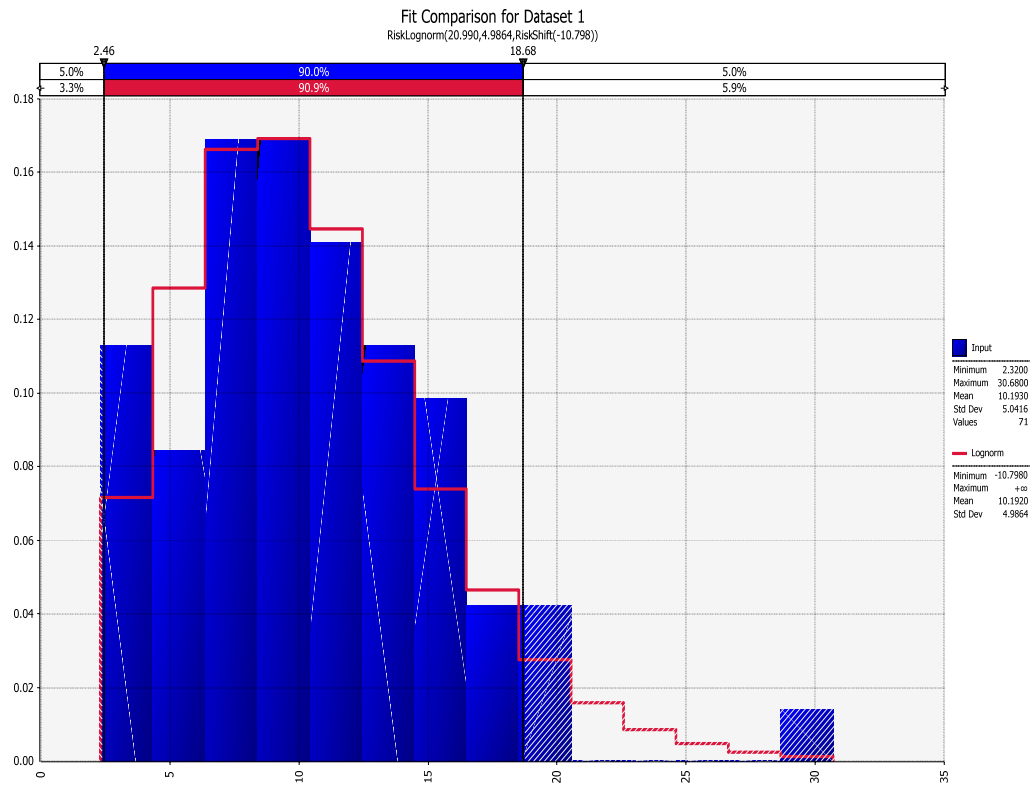


Figure 4.2 Log normal distribution of Young's Modulus. [3]

To represent the main characterization of rock mechanics input parameters in geomechanics determination, the scenarios are designed to select value of concerned variables from the statistical region of $\mu \mp 2 stdv$.

In this regards, the full effect on rock strength properties will be tested on simulation model. The induced stress near wellbore will be observed

correspondingly. As a result, the proposed scenario is summarized and tabulated in Table 4.1

Table 4.1 The Scenario Proposed to Input in Simulation.

Scenario	Cohesion Force (Psi)	Angle of internal friction (degree)	Poisson Ratio	Young Modulus (Psi)
	C_o (Mean $\mu=1497.31$; stdv. =576.91)	ϕ (Mean $\mu =29.87$; stdv. = 6.64)	ν (Mean $\mu = 0.28$; stdv. = 0.068)	E (Mean $\mu =1,477,550$; stdv. = 722,100)
Case 1(base case; Mean)	1497.31	29.87	0.28	1,477,550
Case 2 (varied C_o ; Mean-SD)	920.40	29.87	0.28	1,477,550
Case 3 (varied C_o ; Mean -2SD)	343.49	29.87	0.28	1,477,550
Case 4 (varied C_o ; Mean +SD)	2074.23	29.87	0.28	1,477,550
Case 5 (varied C_o ; Mean +2SD)	2651.14	29.87	0.28	1,477,550
Case 6 (varied ϕ ; Mean-SD)	1497.31	23.23	0.28	1,477,550
Case 7 (varied ϕ ; Mean -2SD)	1497.31	16.59	0.28	1,477,550
Case 8 (varied ϕ ; Mean +SD)	1497.31	36.51	0.28	1,477,550
Case 9 (varied ϕ ; Mean +2SD)	1497.31	43.15	0.28	1,477,550
Case 10 (varied ν ; Mean-SD)	1497.31	29.87	0.21	1,477,550
Case 11 (varied ν ; Mean -2SD)	1497.31	29.87	0.144	1,477,550
Case 12 (varied ν ; Mean +SD)	1497.31	29.87	0.35	1,477,550
Case 13 (varied ν ; Mean +2SD)	1497.31	29.87	0.42	1,477,550
Case 14 (varied E ; Mean-SD)	1497.31	29.87	0.28	755,450
Case 15 (varied E ; Mean -2SD)	1497.31	29.87	0.28	33,350
Case 16 (varied E ; Mean +SD)	1497.31	29.87	0.28	2,199,650
Case 17 (varied E ; Mean +2SD)	1497.31	29.87	0.28	2,921,750

4.2 Failure Criterion for study

Sand production failure model is developed based on Mohr-Coulomb failure model [7] as mentioned in section 3.3 previously. For sandstone formation, it will exhibit friction along a shear plane as the grinding action will restrict motion. The cohesive strength (τ_o) reflects the degree of cementation of the material.

Then Eq. 3.3.1 and 3.3.2 and 3.3.3 are rearranged to normalize for a boundary condition as

$$\sigma'_1 = 2\tau_o \frac{\cos \phi}{1 - \sin \phi} \quad (3.21)$$

Note that σ'_1 is the effective principle stress and τ_o is the cohesive force.

4.3 Reservoir Simulation Model

A finite element method (FEM) is used to calculate the stresses. Eclipse (E300) is able to handle not only a composite fluid but also having a capability to include geomechanics calculation.

The finite element method retains second order accuracy when the grid is skewed. Shear failure can be described a plasticity model under a finite element calculation. Either Mohr-Coulomb or Drucker-Praeger failure criteria can be chosen with or without hardening.

Initial in-situ stress field induced from overburden plus gravity, or tectonic boundary stresses, or thermal effect can be simulated separated or as a whole.

The finite element stress calculation is in cooperating with grid section. The porosity-stress relationship is specifying for RVBAL the rock volume be conserved or the rock mass be approximately conserved RMBAL or the porosity is determined

from a ROCKCOMP model as RCOMP. However in this study the default as RVBAL

The simulation model consists of six main sections as follows:

- Grid section
- PVT section
- SCAL section
- Initialization section
- Schedule section
- Wellbore selection

4.3.1 Grid Section

The grid section is the section used to set basic reservoir geometry and rock properties. The reservoir size, grid block size, number of cells, porosity and permeability are set in this section. A 3D-catesian grid model is used to represent a hypothetical homogeneous reservoir. The grid geometry and properties are illustrated in Table 4.2.

Table 4.2 Grid Geometry and Properties

Description	Value
Reservoir size	1065x1065x1 ft ³
Grid geometry	
Number of cells	25x25x1
X grid block size	100,50,10,5,1 feet
Y grid block size	100,50,10,5,1 feet
Z grid block size	1 feet
Properties	
Porosity	23%
X permeability	20 mD
Y permeability	20 mD
Z permeability	2 mD

Table 4.3 Geomechanics/Solid

Description	Value
Rock Density of Rock stress Balance	146.7 lb/ft ³
Young's Modulus for Rock/ Stress Balance	1.48 x 10 ⁶ Psi
Poisson's Ratio for Rock/ Stress Balance	0.28
Boit's Constant for Rock/Fluid interaction	1

4.3.2 PVT and fluid section

The PVT section is used to input fluid properties, initial temperature, water compressibility and formation compressibility. This study uses ECLIPSE E300 in which fluid properties are set in term of composition. Actual PVT obtained from a sample well called P-01 from onshore Thailand. The initial reservoir temperature is set at 284°F at depth of 5,150 feet representing a typical oil reservoir at onshore of Thailand.

The phase equilibrium is obtained via Peng-Robinson's equation of state. Table 4.4 shows physical properties of each component which are used in the equation of state.

Table 4.4 Fluid composition of well P-01

Component	MW	Overall Composition
CO2	44.0	0.09%
N2	28.0	0.47%
C1	16.0	15.41%
C2	30.1	1.32%
C3	44.1	0.17%
IC4	58.1	0.06%
NC4	58.1	0.06%
IC5	72.2	0.00%
NC5	72.2	0.00%
C6	84.0	0.00%
C7+	225.0	82.42%

4.3.3 SCAL (Special Core Analysis) section

The simulation model uses 3-phases relative permeability for oil/water/gas system. Water saturation function, gas saturation function and oil saturation function used in study are shown in Tables 4.5 to 4.6 and Figures 4.3 to 4.4, respectively.

It is noted that k_{rg} is relative permeability to gas and k_{rw} is relative permeability to water.

Table 4.5 SWOF: Water / Oil Saturation Functions

Sw	Krw	Kro
0.00	0.00	1.00
0.50	0.00	0.13
0.56	0.00	0.09
0.61	0.00	0.06
0.67	0.01	0.04
0.72	0.04	0.02
0.78	0.10	0.01
0.83	0.20	0.00
0.89	0.37	0.00
0.94	0.62	0.00
1.00	1.00	0.00

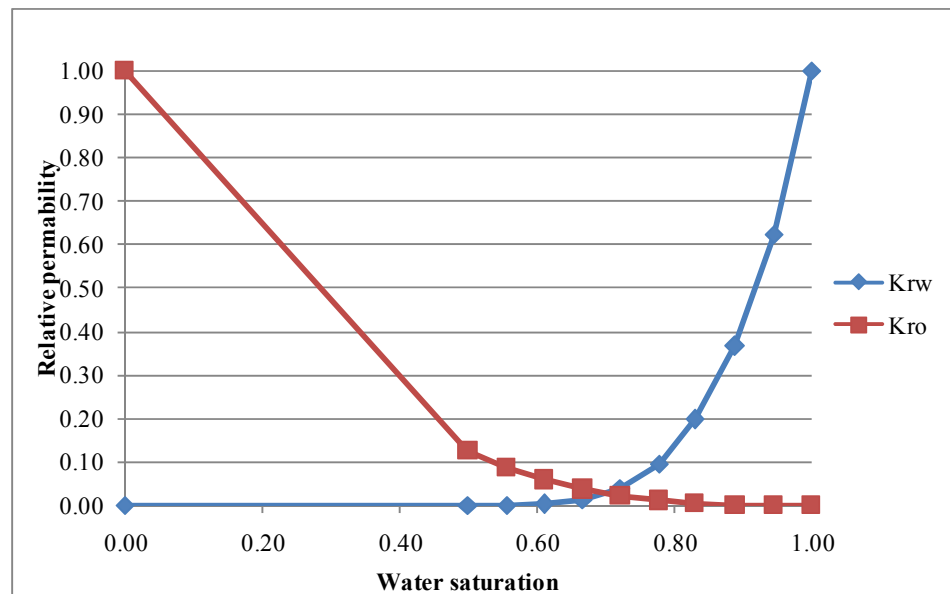


Figure 4.3 Water/Oil saturation function

Table 4.6 SGOF: Gas/Oil Saturation Functions

S_g	K_{rg}	K_{ro}
0.00	0.00	1.00
0.10	0.00	0.81
0.20	0.00	0.64
0.30	0.00	0.49
0.40	0.00	0.36
0.50	0.01	0.25
0.60	0.02	0.16
0.70	0.05	0.09
0.80	0.11	0.04
0.90	0.22	0.01
1.00	1.00	0.00

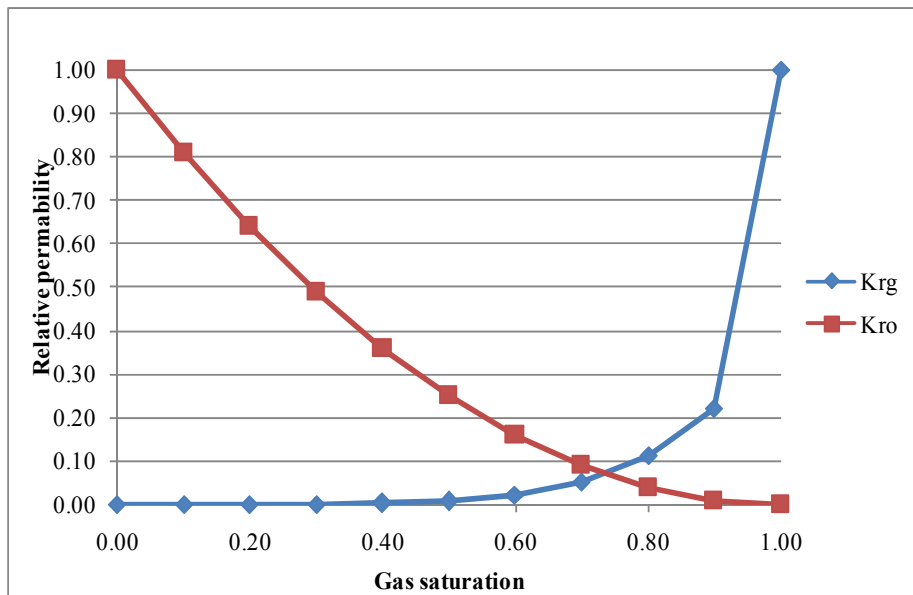


Figure 4.4 Gas/Oil saturation function

4.3.4 Initialization section

Initialization section is used to specify the initial conditions of the model. Three main parameters are defined in this section:

- 1) Datum depth
- 2) Water-oil contact (WOC) depth
- 3) Initial reservoir pressure at datum depth

Datum depth and water-oil contact are specified depth at 5,100 and 5,250 feet, respectively. The initial reservoir pressure is fixed at 1,800 psi. The critical drawdown is obtained from sensitivity of rock strength parameters at failure condition.

4.3.5 Schedule section

This section specifies the well specifications which are well bore inside diameter, perforation interval, production target and bottom hole pressure (BHP) target as shown in Table 4.7.

Table 4.7 Well Specification

Description	Value
Well bore inside diameter	8 3/4"
Perforation interval	feet
Oil production target	200-1,000 BBL/day
BHP target	100 psi

The simulation model has a single well which is set the oil production target 1,000 BBL/day and the minimum bottom-hole pressure of 100 psi.

4.3.6 Wellbore Section

The production well in this study has casing outside diameter of 7 inches with an inside diameter of 6.184 inches. The perforation interval is from the top to the bottom of the reservoir and the interest open hole section is set at 1 foot since the study is focused on a horizon stress against critical flow rate.

4.4 Geomechanics Input Parameters

A base case model is constructed in the simulator model. A based well called P-01 is created in simulator E300 to observe stress near wellbore for drawdown pressure sensitivity. The base case well was setup as follows:

Table 4.8 Geomechanics Input Parameters

Description	Value
Rock density	146.7 lb/ft ³
Top of perforation	5,150 ft
OWC depth	5,250 ft
Initial reservoir pressure	1,800 psi
Target BHP	100 psi
Boundary principle stress X	3,500 psi
Boundary principle stress Y	3,500 psi
Boundary principle stress Z	N/A
Overburden pressure	4,000 Psi
Failure criterion keyword	Mohr Coulomb "MC"
<ul style="list-style-type: none"> • Cohesion 	1,497 psi
<ul style="list-style-type: none"> • Internal friction angle 	29.86 degree
Rock compressibility keyword	RVBAL

CHAPTER V

RESULTS AND DISCUSSIONS

The reservoir volume of $1065 \times 1065 \times 1 \text{ ft}^3$ is discretized by $25 \times 25 \times 1$ grid blocks as seen in Figure 5.1-5.2. The study cases are run with geomechanics input and factory according to the provided information. The study cases are listed out and observed an operation accordingly

In this study, the production well is constructed at the center of the sandstone formation of $X \times Y \times Z$ Cartesian grid coordinate blocks. This well is called P-01 well located at the center of grid block at coordinate (13, 13, 1).

The simulator reports stress parameters for each grid. The stress changes of grid near wellbore is observed as shown in Figures 5.1 – 5.2. The normal stress (x, y, z direction) and the normal shear stress in 3D (xy, yz, zx plane) reporting from simulator are fill in Applet program to calculate a maximum principle stress and minimum principle stress. Then, the Mohr's circles for all directions are constructed, and it will later be compared to the Mohr's failure envelope line.

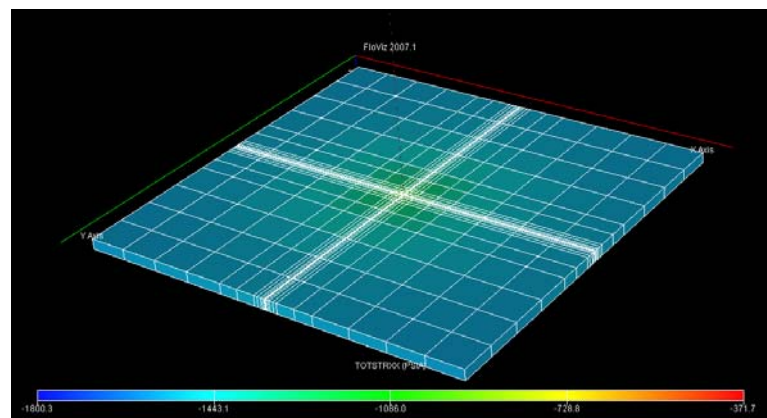


Figure 5.1 Grid model of base case from FloViz simulator modeling

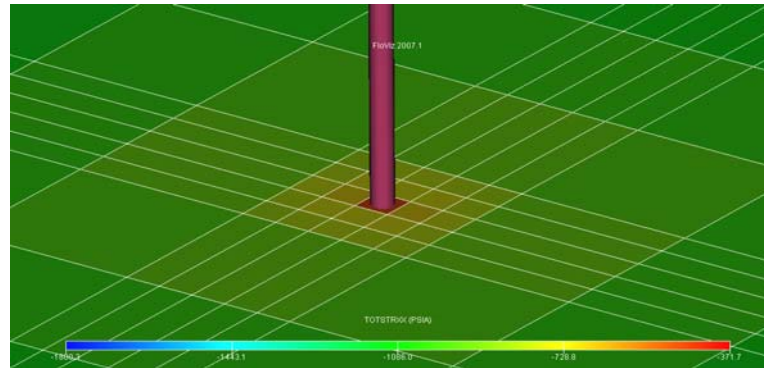


Figure 5.2 Zoom in grid near wellbore from FloViz

The induced stresses as represented by Mohr's circle were superimposed on the Mohr's failure envelope line. The Mohr's failure envelope line generated from the Triaxial test data (cohesion and friction angle) served as a failure criteria to the state of stress at the observed grid block.

5.1 Base case scenario (Case 1)

The mean values of rock strength parameters (C_o , ϕ , ν , E) are input into the model. This model is defined as a base case model. The base case rock strength parameter input for C_o , ϕ , ν , and E are 1497.31 psi, 29.87 degree, 0.28, and 1,477,550 psi, respectively. (Table 5.1)

Table 5.1 Base Case (case 1)

Scenario	Cohesion Force (Psi)	Angle of internal friction (degree)	Poisson's ratio	Young's modulus (Psi)
	C_o	ϕ	ν	E
Case 1 (base case; Mean)	1497.31	29.87	0.28	1,477,550

5.1.1 Results and discussions for case 1:

The observed block locates at grid coordinate (13, 12, 1) represented in a yellow block which is next to well location (P-01) at grid coordinate (13, 13, 1) represented in the grey block as shown in Figure 5.3.

-868.51	-841.12	-868.51
-782.73	-559.40	-782.73
-868.52	-841.13	-868.52
Total normal stress X		
-35.99	-46.27	-35.99
0.00	0.00	0.00
36.00	46.28	36.00
Total shear stress YZ		

-868.51	-782.72	-868.51
-841.13	-559.40	-841.13
-868.52	-782.73	-868.52
Total normal stress Y		
-35.99	0.00	-35.99
-46.27	0.00	-46.27
-35.99	0.00	-35.99
Total shear stress ZX		

-857.95	-779.70	-857.95
-779.71	-469.87	-779.71
-857.95	-779.71	-857.95
Total normal stress Z		
20.56	0.00	-20.56
0.00	0.00	0.00
-20.56	0.00	20.56
Total shear stress XY		

Figure 5.3 Grid coordination reported stresses near wellbore (time step 0.1 days)

From simulation results, the calculated total normal stress in X, Y, Z direction and total shear in XY, YZ, XZ direction (Figure 5.4) are exported to Applet program to plot the 3D Mohr-Coulomb circle. The results of maximum principle stress (σ_1), and minimum principle stress (σ_3) derived in 3D plane are shown in Figure 5.4

The rock strength parameters (C_0 , ϕ) obtained from multiple Triaxial test are used to construct the Mohr's failure envelope line. It serves as a failure criteria to the state of stress at the observed grid block. The induced stresses, generated from the simulation model and represented by Mohr-Coulomb circle, is superimposed on Mohr's failure envelope line. The Mohr's failure envelope line divides the stress field into two zone; stable and unstable zone where the induced stresses filed exceed the formation available strength; therefore a note of formation failure. It is noted that the region above a Mohr's failure envelope line is called an unstable zone. The region under a Mohr's failure envelope line is called a stable zone where the induced stresses field is less than the available formation strength there for no failure occurs.

From Figure 5.4, the Mohr-Coulomb circle does not move across the Mohr's failure envelope to an unstable zone at time step 0.1 days. This base case is categorized as failure case since no sand movement has occurred according to the Mohr-coulomb failure criterion.

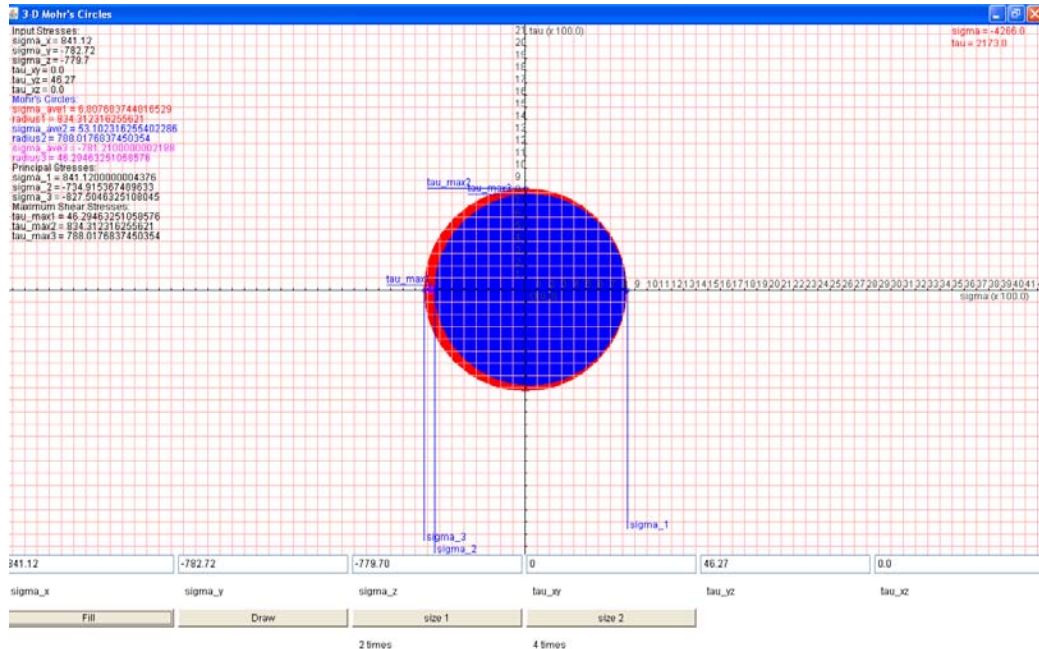


Figure 5.4 Mohr's circle and failure envelope line after case 1 (base case)

In addition, drawdown pressure and oil rate (time step 0.1 days) are reported as a reference for the state of comparison to other cases.

Table 5.2 Drawdown Pressure and Oil Rate Near Wellbore (base case)

Drawdown (psi)	Oil rate (STB/day/ft)
259.52	0.15

Note that in this study, it is assumed that the oil rate represents the oil rate per /formation foot per day,

5.2 Sensitivities of Scenario Cases 2 to Case 17

Sixteen cases (cases 2 to 17) were generated accounting for the statistical variation of the selected variables (C_o , \emptyset , ν , E) covering the distribution area of $\mu \mp 2 \text{ stdv}$. as shown in Table 5.3.

Table 5.3 Sensitivity Cases 2 - 17

Scenario	Cohesion Force (Psi)	Angle of internal friction (degree)	Poisson Ratio	Young Modulus (Psi)
	C_o	\emptyset	ν	E
Case 2 (varied C_o ; Mean-SD)	920.40	29.87	0.28	1,477,550
Case 3 (varied C_o ; Mean -2SD)	343.49	29.87	0.28	1,477,550
Case 4 (varied C_o ; Mean +SD)	2074.23	29.87	0.28	1,477,550
Case 5 (varied C_o ; Mean +2SD)	2651.14	29.87	0.28	1,477,550
Case 6 (varied \emptyset ; Mean-SD)	1497.31	23.23	0.28	1,477,550
Case 7 (varied \emptyset ; Mean -2SD)	1497.31	16.59	0.28	1,477,550
Case 8 (varied \emptyset ; Mean +SD)	1497.31	36.51	0.28	1,477,550
Case 9 (varied \emptyset ; Mean +2SD)	1497.31	43.15	0.28	1,477,550
Case 10 (varied ν ; Mean-SD)	1497.31	29.87	0.21	1,477,550
Case 11 (varied ν ; Mean -2SD)	1497.31	29.87	0.144	1,477,550
Case 12 (varied ν ; Mean +SD)	1497.31	29.87	0.35	1,477,550
Case 13 (varied ν ; Mean +2SD)	1497.31	29.87	0.42	1,477,550
Case 14 (varied E ; Mean-SD)	1497.31	29.87	0.28	755,450
Case 15 (varied E ; Mean -2SD)	1497.31	29.87	0.28	33,350
Case 16 (varied E ; Mean +SD)	1497.31	29.87	0.28	2,199,650
Case 17 (varied E ; Mean +2SD)	1497.31	29.87	0.28	2,921,750

5.2.1 Result and discussion for Cases 2 to 5

For these cases, the sensitivities of cohesion force is tested while the other strength parameters (C_0 , ϕ , ν , E) remains constant at mean value following the rock strength input parameters as described in Table 5.3. The plot of Mohr's circle against Mohr's failure envelope line are shown in Figure 5.5

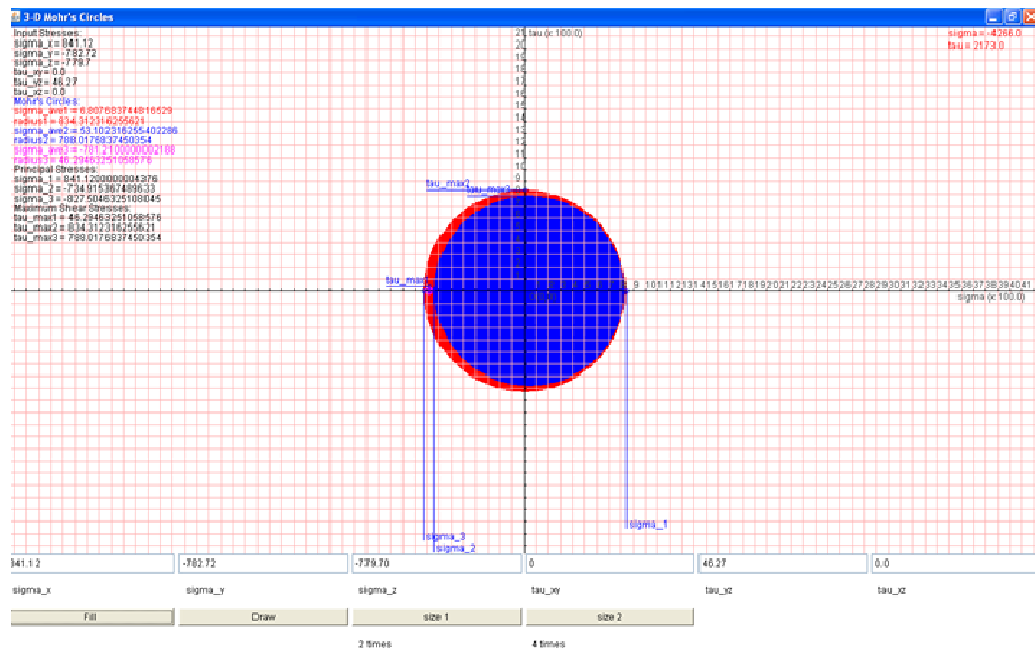


Figure 5.5 Mohr's circle and failure envelope line after cases 2 to 5.

For this case, the sensitivities of cohesion force has significant effect to sand failure evidence is case 2 and 3, the Mohr's circles intersect with the Mohr's failure envelope line. It is suggested that the grid near wellbore at well position (13, 12, 1) became unstable at time step 0.1 days.

In case 2, when the cohesion strength of failure envelope line draws across the cohesion strength of 920 psi ($\mu - stdv.$), then observing the partially intersection between Mohr's circle of principle stresses and failure envelope line. It can be stated that the sand failure most likely to occur at this case.

In case 3, when the cohesion strength of failure envelope line adopt the weakest cohesion strength of 343.49 psi (as the weakest of $\mu - 2 stdv.$), thus lowering the failure envelope line resulted in the intersection between Mohr's circle of principle stresses and failure envelope line. At this point, it is confirmly acknowledged that sand movement has occur.

Case 4 and 5 when cohesion strength of failure envelope line becomes greater, at $\mu + stdv.$ and $\mu + 2 stdv.$, it is clearly demonstrated that the sandstone formation still within the stable zone as no sand movement has occur.

5.2.2 Result and Discussions for Case 6 to 17

For these cases, the sensitivity of internal friction angle, Poisson's ratio and Young's modulus are tested following the rock strength input parameters as described in Table 5.5. It was found that there is a noticeable gap between the Mohr's failure envelope line and Mohr's circle for all cases as the Mohr's circle still located in the stable zone.

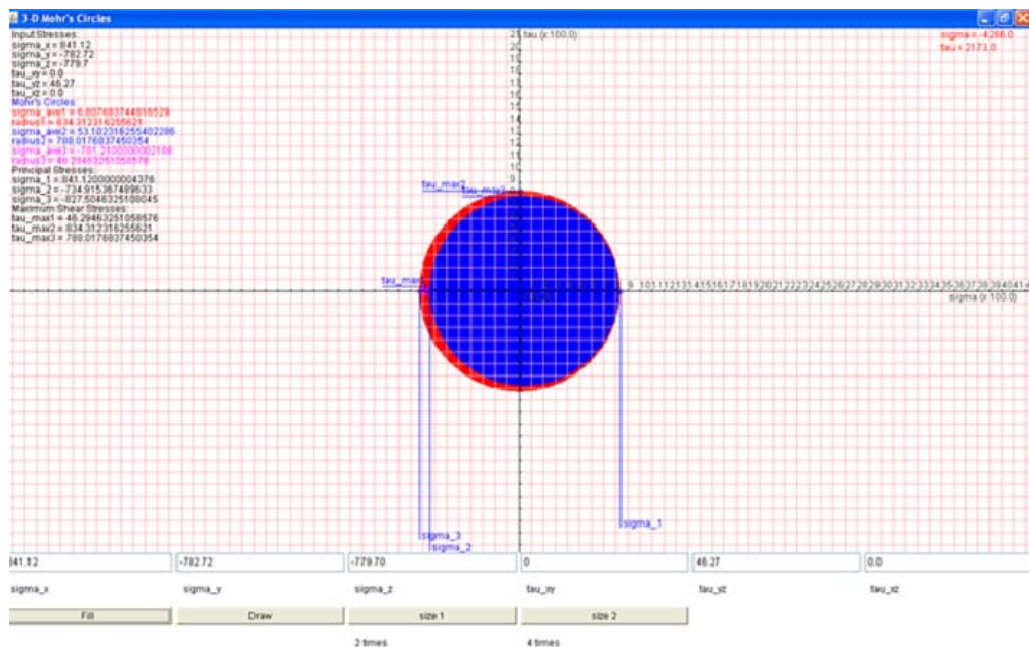


Figure 5.6 Mohr's circle and failure envelope line after cases 6 to 17.

It is clearly stated that the grid near wellbore at well position (13, 13, and 1) still in a stable condition since time step 0.1 days for case 6 to 17. The general conclusion can be draw here that the internal friction angle, Poisson's ratio and Young's modulus have insignificant effect to the stability of the observation block thus no produce failure cases.

5.3 Combination of Minimum Rock Mechanics Parameters from Data

For this case, the minimum values of rock mechanic strength data is selected for all rock strength parameters. The minimum values for cohesion, internal friction angle, Poisson's ratio, and Young's modulus are 812 psi, 20.80 degree, 0.14 and 336,487 psi, respectively (Table 5.4). It is important to note that the failure mechanism of reservoir layer is likely to initiate at the weakest location. Therefore, it is of our interest to run the sensitivity test on the threshold of the minimum values of these concerned rock strength parameters.

Table 5.4 Case at Minimum rock Strength Parameters

Scenario	Cohesion Force (Psi)	Angle of internal friction (degree)	Poisson Ratio	Young Modulus (psi)
	C_0	\emptyset	ν	E
Case Minimum Rate (Q) = 0.102 STB	812	20.80	0.14	336,487

From the simulation results, it is observed that the magnitude of total normal stress at block coordinate (13, 12, 1) varied from 787.96-869.62 psi I x, y, z direction. While the total normal shear stress is recorded 58.48 psi in YZ plane compared in Figure 5.11. The stresses near wellbore are shown in the Figure 5.7.

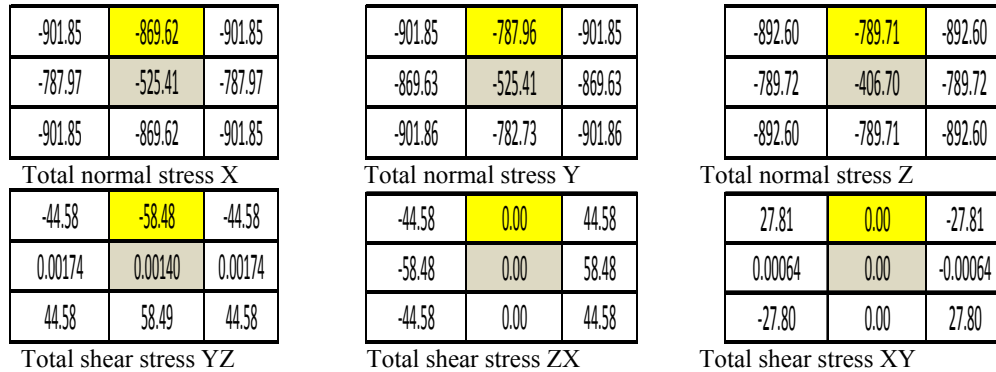


Figure 5.7 Grid coordination reported stresses near wellbore at time step 0.1 days.

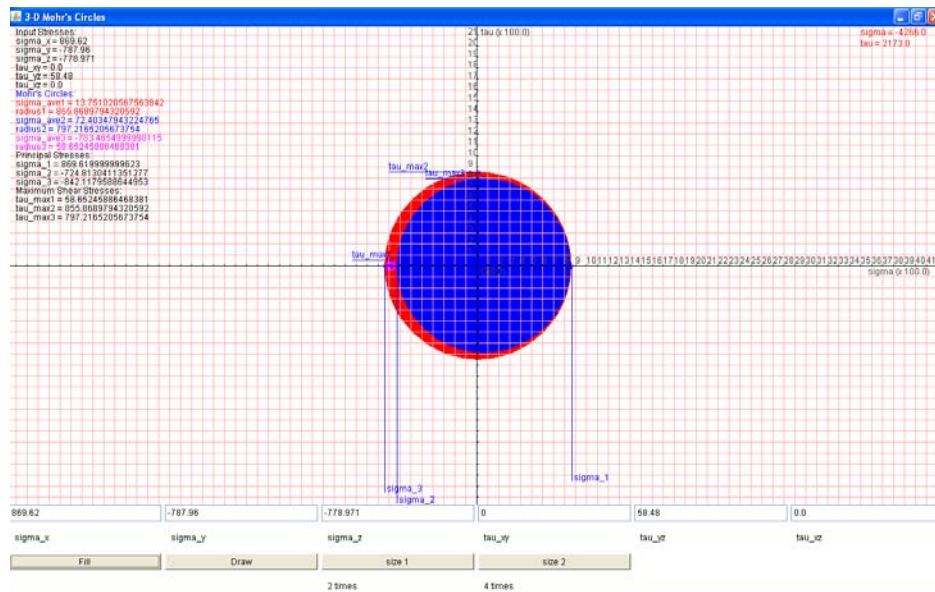


Figure 5.8 Mohr's circle and failure envelope line after case Minimum.

In this case, the cohesion strength of failure envelope line adopt the cohesion strength of 812 psi, thus it results in the intersection of Mohr's circle of principle stress and failure envelope line. At this point, it is clearly demonstrated that sand movement has occur under the minimum values of rock strength data input as seen in Figure 5.8.

The Mohr's failure envelope line at the cohesion strength of 812 psi supports the assumption that the formation has a confirm of sand movement when cohesion in dynamic condition is registered below 812 psi as shown in Figure 5.9.

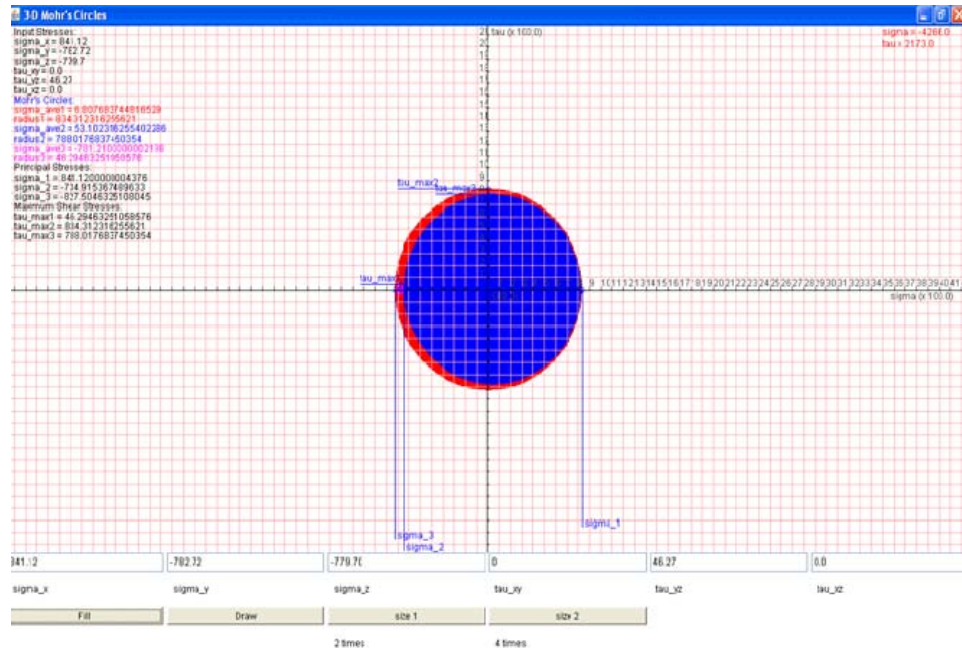


Figure 5.9 Mohr's circle and failure envelope line after cases 2 - 3 against case: Minimum.

5.4 Combination of the Weakest Rock Mechanics Parameters from Data

As the weakest case, the rock strength parameters are adopted at the lower tail distribution at $\mu - 2\text{stdv.}$ with exception of Young's modulus taken as $\mu - 2\text{stdv.}$ since the $\mu - 2\text{stdv.}$ of Young's modulus presents unusual low value at only 33,350 psi.

The input parameter for this case is presented in Table 5.5.

Table 5.5 Case at the Weakest Rock Mechanics Input Parameters

Scenario	Cohesion Force (psi)	Angle of internal friction (degree)	Poisson Ratio	Young Modulus (psi)
	C_0	ϕ	ν	E
Case: Weakest	343.49	16.59	0.12	755,450

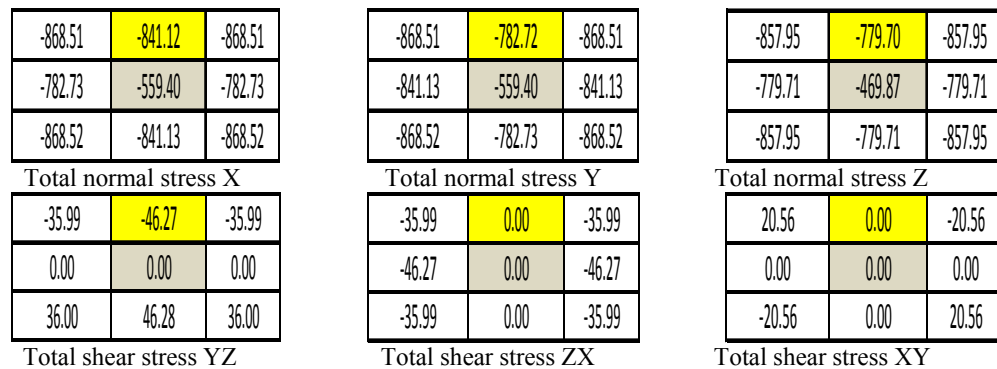


Figure 5.10 Grid coordination representing total normal stress and total shear stress from the case: weakest

From the simulation results, it is observed that the magnitude of total normal stress at block coordinate (13, 13, 1) are varied from 779.70 to 841.12 psi in x, y, z direction. While the total normal stress is recorded at 46.23 psi in YZ plane (Figure 5.10).

For this case, the Mohr's circle moves across the minimum of Mohr's failure envelope line to an unstable zone at time step 0.1 days. At the observed grid coordinate (13, 12, 1) the total normal stress in X, Y, and Z direction are recorded at 841.12, 782.72 and 779.70 respectively. The total shear in YZ plane is recorded at 46.27 psi, while no shear produces in ZX and XY plane.

A Mohr's failure envelope line is selected for both minimum cohesion and internal friction angle (343.49 psi, $\theta = 16.59$ degree) From Figure 5.11 it is clear that the state of stress represented on Mohr's circle is greater than the rock strength represented on Mohr's failure envelope line. This means the observed block is fallen into the unstable zone and expected to produce sand into wellbore.

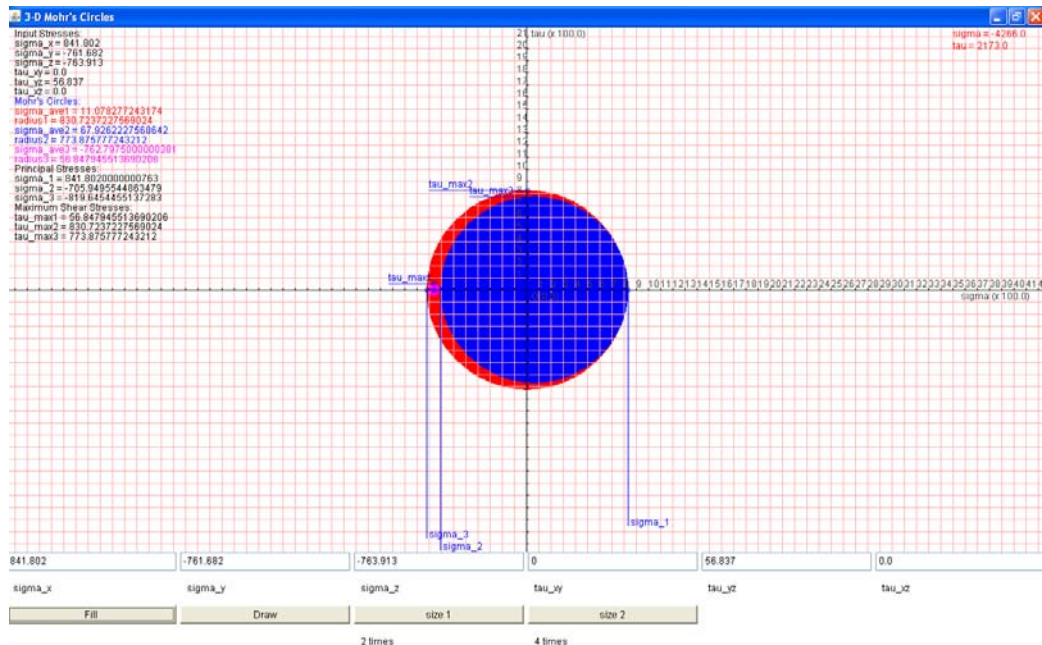


Figure 5.11 Mohr's circle and failure envelope line after adopting the weakest rock mechanics input parameters

5.5 Effect of Reservoir Pressure

The normal stress and shear stress near wellbore. A drawdown is used to monitor changes in the stress around the wellbore. For base case, oil rate of 0.15 STB/day/ft of pay zone results in a drawdown of 259 psi. When the reservoir pressure is 1000 psi and the oil rate is 18.9 STB/day/ft, the resulting drawdown is 106 psi. When the reservoir pressure is increased to 2500 psi and the flow rate is 0.03 STB/day/ft, the drawdown becomes 313 psi. The drawdown increases as the reservoir pressure increases but the oil rate acts in the opposite fashion as shown in Table 5.6.

Table 5.6 Observation of well performance setting oil rate 200 bpd; K =20 mD

Reservoir Pressure (psi)	1000	1800	2500
Oil rate (STB/day/perf-ft)	18.9	0.15	0.03
Drawdown (psi)	106	259	313

At observed grid coordinate (13, 13, 1); the induced total normal stress in X direction is extracted from comparison. As reservoir pressure increases as 1000, 1800, and 2,500 psi respectively. The induced total normal stresses are results as 573.66, 841.80, and 1,125.60 psi accordingly.

-580.15	-573.66	-580.15	-872.92	-841.80	-872.92	1171.42	-1125.60	1171.42
-510.60	-310.60	-510.60	-761.69	-508.54	-761.69	1007.49	-634.32	1007.49
-580.14	-573.66	-580.14	-872.92	-841.81	-872.92	1171.44	-1125.62	1171.44

Total normal stress X (1000 psi) Total normal stress X (1800 psi) Total normal stress X (2500 psi)

Figure 5.12 Grid coordination representing total normal stress in X direction from simulator of reservoir pressure 1000, 1800, 2500 Psi.

The total normal stress near the wellbore increases 33.7% when the reservoir pressure increases 700 psi (from 1,800 to 2,500 psi). The total normal stress near the wellbore decreases 31.8% when the reservoir pressures decreases 800 psi (from 1,800 to 2,500 psi). It is explained that stress will effect to oil rate and drawdown. However capability of oil flowing under low permeability ($K = 20$ mD) is low. The oil rate of higher reservoir pressure will decrease and drawdown will increase accordingly.

5.6 Effect of Reservoir Permeability

In order to investigate the effect of reservoir permeability on the induced stresses, the permeability is varied from 20 mD to 200 mD. The oil rate are varied from 0.03 to 5.5 STB/day/perf-ft. The observed drawdown is varied from 307 to 549 psi as shown in Table 5.7.

Table 5.7 Observation of well performance comparing $K=20$ mD; $K=200$ mD

Reservoir Pressure 1800 psi	K=20 mD	K=200 mD
Oil rate (STB/day/perf-ft)	0.03	5.5
Drawdown (psi)	307	549

At grid block (13, 12, 1) near wellbore, total normal stress increase from 841 psi to 975 psi when the permeability increase from 20 mD to 200 mD. From Figure 5.12, selection at grid coordination in yellow block (13, 12, 1) next to well P-01 position in grey block (13, 13, 1), the maximum principle stress (σ_1), and minimum principle stress (σ_3) are derived in 3D plane.

The results for K=200 mD case are illustrated in Figure 5.13. It is interesting to note that the total stresses near wellbore for case of K=20 mD is different from that for case of K = 200 mD. The case with K = 200 mD shows higher total normal stress than the case with K = 20 mD in all directions.

The total normal stress near the wellbore increases 15% when the permeability (K) increases 10 times from 20 to 200 mD. When Mohr's circles of the two cases are overlaid on the same plot, the one for K = 200 mD is present a bigger Mohr's circle, thus generally more induced stresses as seen in Figure 5.13.

-993.55	-975.06	-993.55	-868.51	-935.69	-993.55	-986.44	-933.66	-986.44
-935.69	-785.25	-935.69	-841.13	-785.25	-975.06	-933.66	-724.92	-933.66
-993.55	-975.06	-993.55	-868.52	-935.69	-993.55	-986.44	-933.66	-986.44
Total normal stress X			Total normal stress Y			Total normal stress Z		
-24.25	-31.18	-24.25	-24.25	-0.00027	24.25	13.85	0.000078	-13.85
0.00	0.00	0.00	-31.18	-0.00030	31.18	0.00	0.00	0.00
24.25	31.18	24.25	-24.25	-0.00027	24.25	-13.85	-0.000078	13.85
Total shear stress YZ			Total shear stress ZX			Total shear stress XY		

Figure 5.13 Grid coordination reported stresses near wellbore at time step 0.1 days for K = 200 mD

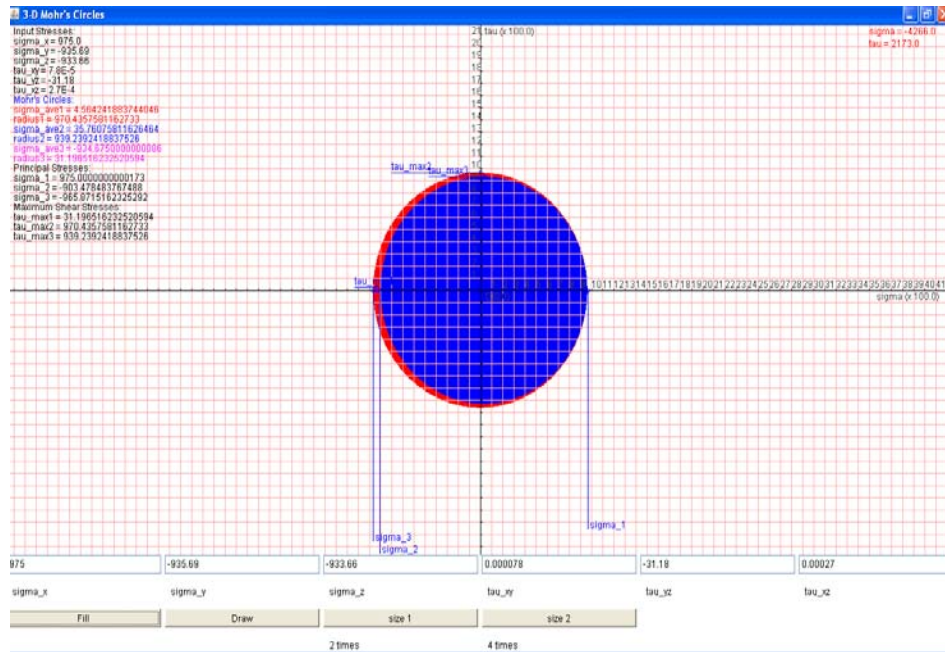


Figure 5.14 Schematic representing case $K = 20$ mD and $K = 200$ mD

CHAPTER VI

CONCLUSIONS AND RECOMMENDATIONS

6.1 Conclusions

This chapter summarizes the effects of rock mechanics parameters (cohesion force, internal friction angle, Poisson's ratio, and Young's modulus), reservoir pressure and permeability, on the estimation of induced stresses when the reservoir has potentially approach rock failure condition and consequently sand production. Recommendations for further study are also included.

First, in view of rock strength variation, it can be concluded that the variation of all rock strength parameters has less effect on stress changes around wellbore in almost every scenario. As evidence that the total normal and shear stresses varies within the narrow range of 767 to 869 psi and 46.13 to 46.27, respectively.

The rock mechanics parameters are varied and the total normal stresses around wellbore were observed as followed.

- **Cohesion force.** This parameter is varied from 343.49 to 2651.14 psi. The result of total normal stresses at grid around wellbore are ranging between 787 to 869 psi.
- **Angle of internal friction.** This parameter is varied from 16.59 degree to 43.15 degree. The result of total normal stresses at grid around wellbore are ranging between 787 to 869 psi.
- **Poisson Ratio.** This parameter is varied from 0.14 to 0.42. The result of total normal stresses at grid around wellbore are ranging between 787 to 869 psi.
- **Young modulus.** This parameter is varied from 33,350 psi to 2,921,750 psi. The result of total normal stresses at grid around wellbore are ranging between 787 to 869 psi.

From the rock strength parameters input point of view, the cohesion can be draw that the sensitivities of cohesion force has significant effect to sand failure. The sand movement is likely to initiate when the cohesion strength reduces to $\mu - stdv.$ at 920 psi. And, the confirmed sand movement is clearly stated when the cohesion strength reduces to $\mu - 2 stdv.$ at 343.49 psi. While the other rock strength parameter, the internal friction angle, Poisson's ratio, and Young's modulus, have insignificant effect to sand movement.

It is important to note that the sandstone formation is subjected to the prior flooding operation and the rock mechanics data used in this study is tested before the flooding operation. The flooding will reduce rock strength especially the cohesion force when the cementing material in the rock matrix weakens. Without information of rock mechanics parameters after flooding, it is rather complicate to identify a cut-off point as the failure condition in the model.

For reservoir pressure variation, the total normal stress near the wellbore increases 33.7% when the reservoir pressure increases 700 psi (from 1,800 to 2,500 psi). The total normal stress near the wellbore decreases 31.8% when the reservoir pressures decreases 800 psi (from 1,800 to 2,500 psi). It is explained that stress will effect to oil rate and drawdown. However capability of oil flowing under low permeability ($K = 20$ mD) is low. The oil rate of higher reservoir pressure will decrease and drawdown will increase accordingly.

For the reservoir permeability variation, the total normal stress near the wellbore increases 15% when the permeability (K) increases 10 times from 20 to 200 mD. When Mohr's circles of the two cases are overlaid on the same plot, the one for $K = 200$ mD is present a bigger Mohr's circle, thus generally more induced stresses

In overall, the most important rock strength parameters in terms of sand failure prediction are the cohesion strength. The results of this study indicate that the cohesion strength below 812 psi provide the possibility of sand failure case. At the

same analysis, the reservoir pressure and permeability show impact to induced stresses near wellbore.

6.2 Recommendations

At the outset of this study some recommendation can be made to further complete this research work.

First, changing the principle stress of boundary condition in simulation model can be investigated in observing the changing of total stresses near wellbore.

Second, the most update core analysis report of infill well can be used to adjust for geomechanics parameters in the model. It will help to calibrate a Mohr's failure envelope line to represent the in-situ condition of formation strength.

Third, the integration of indirect test such as well log data can be used to update the geomechanic model. The empirical relationship between indirect and direct information (data from core test) can be established prior inject to the indirect information into the analytical model.

REFERENCES

- [1] Coated, D.F., Rock mechanic principles, mines branch monograph 874, Ottawa, Ont: Dept. of Mines and Technical Surveys, 1965.
- [2] Stein N., Hilchie D.W. Estimating the maximum production rate possible from friable sandstones without using sand control. Journal of Petroleum Technology Trans., AIME, 253 (September 1972): 1157-1160.
- [3] S1 Asset Team DSP/R. A Conceptual Development Plan of the Prukrathiam Area, PTTEP SIAM, Bangkok, Thailand (2010): 7-11.
- [4] Tingay M., Sirikit Field In-situ Stress Study: Preliminary results, Geophysics Institute, Univ. Karlsruhe, GERMANY, 2010
- [5] Wu B., Tan C.P., Connelly L., Tsaganas S., Camilleri M. and Maney B., CSIRO Petroleum, Compressive Strength, TWC Collapse Pressure and Fracture Toughness Properties of THAI SHELL Cores LKU-E17 report, TSEP Co., Thailand, (September 2001)
- [6] TRACS International, A New interpretation of the Structural Geology of the Sirikit Field Area, PTTEP SIAM, Bangkok, Thailand: (2001):4.
- [7] Brent S. Aadnoy and Reza Looyeh. Petroleum rock mechanics. Gulf Publishing, 2011.
- [8] Hubbert M. K. and Willis D.G. Mechanics of Hydraulic Fracturing”, Presented on Petroleum Fall Meeting in Los Angeles: October 14-17, 1956.
- [9] Nathan and Hilchie D.W. Estimating the maximum production rate possible from friable sandstones without using sand control, (SPE 3499-PA) Journal of Petroleum Technology, (September 1972): 1157-1160.
- [10] Wiesenberger et al, Sand prediction modeling. Journal of Petroleum Technology, 1987
- [11] Kantzas and Rothenberg Determination of stress strain characteristics of sand packs under uniform loads by the use of compute-assisted tomography and finite element modeling (SPE 23791-MS) SPE Formation Damage Control Symposium, Lafayette, Louisiana, 26-27 February 1992.
- [12] Barrett et al. Novel wellbore strengthening enables drilling of exploration well in a highly depleted formation.

- [13] Nouri A., Vanziri H., Belhaj H., Islam R., Sand-Production Prediction: A New set of Criteria for Modeling Based on Large-Scale Transient Experiments and Numerical Investigation Society of Petroleum Engineering Journal, June 2006: 227-237
- [14] Zhang J. and Standifird W.B. Optimized Perforation Tunnel Geometry, Density and Orientation to Control Sand Production (paper SPE 107785), the European Formation Damage Conference, Scheeveningen, the Netherlands, 30 May -1 June 2007
- [15] Bratli R. K. and Risnes R. Stability and Failure of Sand Arches, Journal of Petroleum Technology, SPE-AIME (April 1981): 236-248.
- [16] Risnes R. and Horsrud P. Sand Arching-A Case Study (SPE 12948)
- [17] Morita N., Whitfill D.L. Fedde O.P. Lovik T.H. Parametric study of sand production prediction: analytical approach. SPE Production Engineering 4 (1989b): 25-33.
- [18] Weingarten J.S., and Perkins T.K.. Prediction of sand production in gas wells: Methods and Gulf of Mexico studies. //Journal of Petroleum Technology 47: 596-600.
- [19] Van den Hoek et al. A new concept of sand production prediction: Theory and laboratory experiments. (Paper SPE 65756-PA), Journal of SPE drilling and completion Vol.15, December 2000.
- [20] Stavropoulou M. et al. Sand erosion in axial flow conditions. Klauer Academic Publishers, Netherlands (2001): 267-281
- [21] Papamichos E., Malmanger E.M. A Sand Erosion Model for Volumetric Sand Predictions in A North Sea Reservoir, SPE paper, Journal of Reservoir Evaluation and Engineering, (February 2001): 44-50.
- [22] Hibbitt, ABACUS Theory Manual, Karlsson and Sorensen, Inc, 1998.
- [23] Tippie, D.B., and Kohlhas, C.A. Effect of Flow Rate and Stability of Unconsolidated Producing Sands (paper SPE 4533). SPE-AIME 48th Annual Fall Meeting, Las Vegas, Nev: Journal of Petroleum Technology (September 30-October 3, 1973)
- [24] Burton R.C. L.Y. Chin, Davis E.R., Enderlin M., Fuh G., R. Hodge, G.G. Ramos, P. VanDeVerg, And M. Werner, ConocoPhillips, and W.L. Mathews and S.

Petersen, BP. North Slope Heavy-Oil Sand-control Strategy: Detailed Case Study of Sand Production Predictions and Field Measurements for Alaskan Heavy-Oil Multilateral Field Developments presented in 2005 SPE Annual Technical Conference and Exhibition, Dalas, Texas, USA, (9-12 October, 2005)

[25] Qiu K., Marsden J.R., Alexander J., and Retnanto A., Schlumberger, and O.A. Abdelkarim and Shatwan M., , “ Practical Approach To Achieve Accuracy In Sanding Prediction (paper SPE 100944) presented at the SPE 2008 Asia Pacific Oil & Gas Conference and Exhibition held in Adelaide, Australia, SPE, Amoco (11-13 September 2006):

[26] Amos S. Kim, Mukul M. Sharma and Harvey Fitzpatrick. A Prediction Model for Sand Production in Poorly Consolidated Sands, (Paper IPTC 15087), IPTC conference, Bangkok, Thailand, IPTC (7-9 February 2012).

[27] Hall C.D., Jr. and Harrisberger W.H. Stability of Sand Arches: A Key to Sand Control Journal of Petroleum Technology (July 1970): 821-829.

[28] Stien N., Odeh A.S., Jones L. G. Estimating the Maximum Sand-Free Production Rates From Friable Sands for Different Well Completion Geometries , Journal of Petroleum Technology (Oct. 1974):1156-1158

[29] Lubinski A. Theory of Elasticity for Porous Bodies Displacing a Strong Pore Structure. Proceeding of Second U. S. Notational Congress. Applied Mechanics. American Society of Mechanical Engineers, 1955, (June 1954): 247-256

[30] Cheatham J.B. Jr. Wellbore Stability, Journal of Petroleum Technology (June 1984): 889-896.

[31] Richard M. Bateman Formation Evaluation using Well Logging Measurements. IHRDC, Boston, MA USA: 1986: 145-148

[32] Richard M. Bateman Well Logging Tools and Techniques, IHRDC, Boston, MA USA, 1991: 143-164

[33] Dake L.P., Fundamental of Reservoir Engineering, Elsevier Scientific Publishing Company, Netherlands, 1978.

[34] Khaksar A. and Rahman K. and Ghani J. and Mangor H., Integrated Geomechanical Study for Hole Stability, Sanding Potential and Completion Selection: A case Study from South East Asia, (Paper SPE 115915), the 2008 SPE Annual Conference and Exhibition held in Denver, Colorado, USA, 21-24 September

2008.

[35] L. M. Yeow and Z. Johar and B.Wu and C.Tan and M. A. Yaakub, Sand Production Prediction Study Using Empirical and Laboratory Approach for a Multi-Field Gas Development, Paper SPE 87004 presented at SPE Asia Pacific Conference on Integrated Modelling for Asset Management, KL Malaysia, 29-30 March 2004.

[36] Veeken, C.A. M. D. R. Davies, C.J. Kenter, and A.P. Kooijman (1991): Sand Production Prediction Review: Developing and Integrated Approach, Paper SPE 22792 Presented at the Annual Technical Conference and Exhibition of SPE, DFallas, Texas, 6-9 October 1991.

[37] Kenter C.J. and Currie P.K. Past & Future Contribution of Rock Mechanics Research to Petroleum Engineering (Paper SPE/ISRM 50559), SPE/ISRM EUROCK'98 Conference, Trondheim, Norway, (8-10 July 1998)

APPENDICES

APPENDIX A

A-1) Reservoir model

A single reservoir model (composite oil reservoir) is generated by entering required data into ECLIPSE 300 reservoir simulator. The model used in this study composes of 25 x 25 x 1 blocks in the x-, y- and z- directions.

A-2) Case Definition

Simulator:	Compositional		
Model dimensions:	Number of cells in the x-direction		25
	Number of cells in the y-direction		25
	Number of cells in the z-direction		1
Grid type:	Cartesian		
Geometry type:	Block centered		
Oil-Gas-Water options:	Oil and Gas		
Number of components:	10		
Pressure saturation options (solution type):	IMPES		

A-3) Reservoir properties

Grid

Properties: Active grid blocks:	Oil reservoir		
	X, Y, Z =		25, 25, 1-5
	Source reservoir		
	X, Y, Z =		25, 25, 7-11
Porosity		=	0.23
Permeability	k-x =	20	mD
	k-y =	20	mD
	k-z =	2	mD

X Grid block sizes (All X = 1-25)	=	1,5,10,50,100 ft
Y Grid block sizes (All Y = 1-25)	=	1,5,10,50,100 ft
Z Grid block sizes (for Z = 1)	=	1 ft
Depth of Top face (Top layer)	=	5150 ft

APPENDIX B

B-1) E300 Simulation file Dataset_ (7-May-13).DATA

```

--
-----
-----
-- Office Simulation File (DATA) Data Section Version 2010.2 Oct 15 2010
-----
-----
--
-- File: Dataset_(7-May-13).DATA
-- Created on: 7-May-2013 at: 21:11:37
--
*****
*
-- *                               WARNING
*
-- *               THIS FILE HAS BEEN AUTOMATICALLY GENERATED.
*
-- *               ANY ATTEMPT TO EDIT MANUALLY MAY RESULT IN INVALID DATA.
*
--
*****
*
--

RUNSPEC

TITLE
title

START
  1 'JAN' 2012 /

FIELD

MULTIN

MULTOUT

GAS

OIL

WATER

IMPES

COMPS
  11 /

DOMAIN
  28800 /

NOFREEZE

```



```
NSTACK
 10 /

MONITOR

RSSPEC

NOINSPEC

MSGFILE
 1 /

GEOMECH
1* T FE RVBAL INIT COMPN NOINITH /

GEODIMS
 1 1 1 1 1 /

AQUDIMS
 1 1 2 1 1 1 /

SCFDIMS
 5 3 3 /

DIMENS
 25 25 1 /

SCDPDIMS
 0 0 0 0 1 0 /

EQLDIMS
 1 100 100 1 20 /

REGDIMS
 1 1 0 1 0 1 /

TABDIMS
 1 1 50 50 1 20 20 1 1 1 1 1 1 0 0 1 /

WELLDIMS
 2 21 2 2 5 10 5 4 3 0 1 1 /

GRID

GRIDFILE
 2 /

INIT

ECHO

GRIDUNIT
--
-- Specifies the grid data units
--
```

```

'FEET' /
--
-- Grid Axes wrt Map Coordinates
--
MAPAXES
--
-- Grid Axes wrt Map Coordinates
--
          0          0          0          0          0          0 /
EQUALS

PORO 0.23 /
PERMX 20 /
PERMY 20 /
PERMZ 2 /

DX 100 /
DY 100 /
DZ 1 /

TOPS 5150 1 25 1 25 1 1 /

DX 50 5 21 1 25 1 1 /
DX 10 7 19 1 25 1 1 /
DX 5 9 17 1 25 1 1 /
DX 1 11 15 1 25 1 1 /

DY 50 1 25 5 21 1 1 /
DY 10 1 25 7 19 1 1 /
DY 5 1 25 9 17 1 1 /
DY 1 1 25 11 15 1 1 /

/

--
-- -----
-- Office Grid Properties (GRDPROP) Data Section Version 2010.2 Oct
15 2010
-- -----
--
*****
*****
-- *                               WARNING
*
-- *               THIS FILE HAS BEEN AUTOMATICALLY GENERATED.
*
-- *               ANY ATTEMPT TO EDIT MANUALLY MAY RESULT IN INVALID
DATA.               *
--
*****
*****
--
--
--

```

```

-----
-----
-- Office Grid non-geom, non-prop non-operational non-parallel
keywords (GRDOTHERS) Data Section Version 2010.2 Oct 15 2010
-----
-----
--
--
--
*****
*****
-- *                               WARNING
*
-- *                               THIS FILE HAS BEEN AUTOMATICALLY GENERATED.
*
-- *                               ANY ATTEMPT TO EDIT MANUALLY MAY RESULT IN INVALID
DATA.                               *
--
*****
*****

--
-- File: GEO_MECH_GOTH.INC
-- Created on: 31-Jul-2012 at: 13:13:21
--
--
--
--*BOX panel edit: ROCKDEN set equal to 146.7 lb /ft^3 for box
(1:51, 1:51, 1:20)
EQUALS
ROCKDEN 146.7 /
YOUNGMOD 1477985 /
POISSONR 0.2788 /
BIOTC 1 /
/

PROPS

--
-----
-----
-- Office PVTN (PVTN) Data Section Version 2010.2 Oct 15 2010
-----
-----
--
-- File: BASECASE_GEOMECH_TEST_PVT.INC
-- Created on: 24-Mar-2013 at: 17:40:48
--
--
*****
*****
-- *                               WARNING
*
-- *                               THIS FILE HAS BEEN AUTOMATICALLY GENERATED.
*

```

```

-- *          ANY ATTEMPT TO EDIT MANUALLY MAY RESULT IN INVALID
DATA.          *
--
*****
*****
--
-- OFFICE-PVTN-HEADER-DATA
-- Off PVTN Component Names:          11          1
-- Off PVTN "CO2"
-- Off PVTN "N2"
-- Off PVTN "C1"
-- Off PVTN "C2"
-- Off PVTN "C3"
-- Off PVTN "IC4"
-- Off PVTN "NC4"
-- Off PVTN "IC5"
-- Off PVTN "NC5"
-- Off PVTN "C6"
-- Off PVTN "C7+"
-- Off PVTN PVT Tables:                1          1
-- Off PVTN "PVT 1"
-- Off PVTN EoS Reservoir Tables:      1          1
-- Off PVTN "EoS(Res) 1"
-- Off PVTN Geomechanics Tables:       1          1
-- Off PVTN "Geomechanics 1"
ECHO
--
-----
-----
-- Office PVTN (PVTN) Data Section Version 2010.2 Oct 15 2010
-----
-----
--
-- File: BASECASE_GEOMECH_TEST_PVT.INC
-- Created on: Mar-22-2013 at: 07:03:05
--
--
*****
*****
-- *          WARNING
*
-- *          THIS FILE HAS BEEN AUTOMATICALLY GENERATED.
*
-- *          ANY ATTEMPT TO EDIT MANUALLY MAY RESULT IN INVALID
DATA.          *
--
*****
*****
--
-- OFFICE-PVTN-HEADER-DATA
--
-----
-----
-- Office PVTN (PVTN) Data Section Version 2007.1 May 26 2007
-----
-----
--
-- File: GEO_MECH_PVT.INC

```

```

-- Created on: 28-Jul-2012 at: 11:55:08
--
--
*****
*****
-- *
-- *                               WARNING
-- *
-- *                               THIS FILE HAS BEEN AUTOMATICALLY GENERATED.
-- *
-- *                               ANY ATTEMPT TO EDIT MANUALLY MAY RESULT IN INVALID
DATA.      *
--
*****
*****
--
-- OFFICE-PVTN-HEADER-DATA
--
-- Number of Components
--
NCOMPS
--
-- Number of Components
--
      11
/
--
-- Modified Peng-Robinson EOS
--
--
-- Component Names
--
PRCORR
--
-- Modified Peng-Robinson EoS
--
CNames
--
-- Component Names
--
      'CO2'
      'N2'
      'C1'
      'C2'
      'C3'
      'IC4'
      'NC4'
      'IC5'
      'NC5'
      'C6'
      'C7+'
/
--
-- Lorentz-Bray-Clark Viscosity Correlation Coefficients
--
LBCCOEF
--
-- Lorentz-Bray-Clark Viscosity Correlation Coefficients
--

```

```

    0.1023 0.023364 0.058533 -0.040758 0.0093324
/
ECHO
GRAVITY
--
-- Fluid gravities at surface conditions
--
    39          1      0.7773
/

ECHO
-- Units: F
--
-- Constant Reservoir Temperature
--
-- Initial Reservoir Temperature
--
RTEMP
--
-- Initial Reservoir Temperature
--
    140
/

--
-- Equation of State (Reservoir EoS)
--
EOS
--
-- Equation of State (Reservoir EoS)
--
    PR
/

--
-- Molecular Weights (Reservoir EoS)
--
MW
--
-- Molecular Weights (Reservoir EoS)
--
    44.01
    28.013
    16.043
    30.07
    44.097
    58.123992
    58.124008
    72.150992
    72.151008
    84
    225
/

--
-- EoS Omega-a Coefficient (Reservoir EoS)
--

```

```

OMEGAA
--
-- Overrides default ?a values
--
0.457235529
0.457235529
0.457235529
0.457235529
0.457235529
0.457235529
0.457235529
0.457235529
0.457235529
0.457235529
/

--
-- EoS Omega-b Coefficient (Reservoir EoS)
--
OMEGAB
--
-- Overrides default ?b values
--
0.077796074
0.077796074
0.077796074
0.077796074
0.077796074
0.077796074
0.077796074
0.077796074
0.077796074
0.077796074
/

-- Units: R
--
-- Critical Temperatures (Reservoir EoS)
--
--
-- Critical Temperatures (Reservoir EoS)
--
TCRIT
--
-- Critical Temperatures (Reservoir EoS)
--
548.459999999228
227.160000017685
343.0799999988516
549.774000004037
665.640000033438
734.5799999959724
765.3599999975116
828.7199999953583
845.2799999992273
913.499999999486

```

```

1340.59299801359
/
-- Units: psia
--
-- Critical Pressures (Reservoir EoS)
--
--
-- Critical Pressures (Reservoir EoS)
--
PCRIT
--
-- Critical Pressures (Reservoir EoS)
--
1071.33110996644
492.312649984577
667.78169597908
708.342379977809
615.75820998071
529.052399983426
550.655372982749
491.5778549846
488.785633984687
436.615188986322
232.461979592717
/
-- Units: ft3 /lb-mole
--
-- Critical Volumes (Reservoir EoS)
--
--
-- Critical Volumes (Reservoir EoS)
--
VCRIT
--
-- Critical Volumes (Reservoir EoS)
--
1.50573518513559
1.44166134747024
1.56980902280093
2.37073199361773
3.20369188326721
4.21285482649638
4.08470715116569
4.9336855002315
4.98174087848051
5.62247925513395
14.1948022127846
/
--
-- Critical Z-Factors (Reservoir EoS)
--
ZCRIT
--
-- Critical Z-Factors (Reservoir EoS)
--

```



```

0.274077797373613
0.291151404367252
0.284729476638113
0.284634795098265
0.276164620027245
0.282736958766292
0.27385554910948
0.272710871597912
0.268438914152292
0.250417484943733
0.229366945004871
/
--
-- EoS Volume Shift (Reservoir EoS)
--
SSHIFT
--
-- EoS Volume Shift (Reservoir EoS)
--
-0.04273033674
-0.1313342386
-0.1442656189
-0.103268354
-0.07750138148
-0.06198372515
-0.05422489699
-0.04177245672
-0.03027789648
-0.007288775999
0.1737326679
/
--
-- Acentric Factors (Reservoir EoS)
--
ACF
--
-- Acentric Factors (Reservoir EoS)
--
0.225
0.04
0.013
0.0986
0.1524
0.1848
0.201
0.227
0.251
0.299
0.7316792253
/
--
-- Binary Interaction Coefficients (Reservoir EoS)
--
BIC
--

```

```

-- Binary Interaction Coefficients (Reservoir EoS)
--
-0.012
  0.1    0.1
  0.1    0.1    0
  0.1    0.1    0    0
  0.1    0.1    0    0    0
  0.1    0.1    0    0    0    0
  0.1    0.1    0    0    0    0    0
  0.1    0.1    0    0    0    0    0    0
  0.1    0.1    0.0279    0.01    0.01    0    0    0
0
0
  0.1    0.1    0.049684    0.01    0.01    0    0    0
0
  0
/
--
-- Component Parachors
--
PARACHOR
--
-- Component Parachors
--
  78
  41
  77
  108
  150.3
  181.5
  189.9
  225
  231.5
  271
  581.66675
/
-- Units: ft3 /lb-mole
--
-- Critical Volumes for Viscosity Calc (Reservoir EoS)
--
--
-- Critical Volumes for Viscosity Calc (Reservoir EoS)
--
VCRITVIS
--
-- Critical Volumes for Viscosity Calc (Reservoir EoS)
--
  1.50573518513559
  1.44166134747024
  1.56980902280093
  2.37073199361773
  3.20369188326721
  4.21285482649638
  4.08470715116569
  4.9336855002315
  4.98174087848051
  5.62247925513395

```

```

14.1948022127846
/
--
-- Overall Composition
--
ZI
--
-- Overall Composition
--
0.0009
0.0047
0.1541
0.0132
0.0017
0.0006
0.0006
0
0
0
0.8242
/
--
-- Critical Z-Factors for Viscosity Calculation (Reservoir EoS)
--
ZCRITVIS
--
-- Critical Z-Factors for Viscosity Calculation (Reservoir EoS)
--
0.274077797373613
0.291151404367252
0.284729476638113
0.284634795098265
0.276164620027245
0.282736958766292
0.27385554910948
0.272710871597912
0.268438914152292
0.250417484943733
0.229366945004871
/
ECHO
--
-- Geomechanics Yield Function Parameters
--
GEOYLDF
--
-- Geomechanics Yield Function Parameters
--
1497.31 29.8685 'MC' 2300 'PER'
1 1 /
/
--

```

```

-----
-----
-- Office SCAL (SCAL) Data Section Version 2010.2 Oct 15 2010
-----
-----
--
-- File: BASECASE_GEOMECH_TEST_SCAL.INC
-- Created on: Mar-24-2013 at: 15:30:19
--
--
*****
*****
-- *                               WARNING
*
-- *                               THIS FILE HAS BEEN AUTOMATICALLY GENERATED.
*
-- *                               ANY ATTEMPT TO EDIT MANUALLY MAY RESULT IN INVALID
DATA.                               *
--
*****
*****
--
-- OFFICE-SCAL-HEADER-DATA
--
-----
-- Office SCAL Keywords
-----
--
ECHO
--
-----
-- Office SCAL (SCAL) Data Section Version 2010.2 Oct 15 2010
-----
-----
--
-- File: BASECASE_GEOMECH_TEST_SCAL.INC
-- Created on: Mar-22-2013 at: 01:40:45
--
--
*****
*****
-- *                               WARNING
*
-- *                               THIS FILE HAS BEEN AUTOMATICALLY GENERATED.
*
-- *                               ANY ATTEMPT TO EDIT MANUALLY MAY RESULT IN INVALID
DATA.                               *
--
*****
*****
--
-- OFFICE-SCAL-HEADER-DATA
--
-----
-----

```

```

-- Office SCAL Keywords
-- -----
--
--
-- -----
-- Office SCAL (SCAL) Data Section Version 2007.1 May 26 2007
-- -----
--
--
-- File: GEO_MECH_SCAL.INC
-- Created on: 19-Aug-2012 at: 14:56:02
--
--
*****
*****
-- *                               WARNING
*
-- *                               THIS FILE HAS BEEN AUTOMATICALLY GENERATED.
*
-- *                               ANY ATTEMPT TO EDIT MANUALLY MAY RESULT IN INVALID
DATA.                               *
--
*****
*****
--
-- OFFICE-SCAL-HEADER-DATA
--
-- Water/Oil Saturation Functions
--
SWOF
--
-- Water / oil saturation functions versus water saturation
--
          0          0          1          0
        0.5          0          0.125        0
0.55555556 0.000152416 0.087791495        0
0.61111111 0.002438653 0.058813443        0
0.66666667 0.012345679 0.037037037        0
0.72222222 0.039018442 0.021433471        0
0.77777778 0.095259869 0.010973937        0
0.83333333 0.19753086  0.00462963        0
0.88888889 0.36595031 0.001371742        0
0.94444444 0.62429508 0.000171468        0
          1          1          0          0
/
--
-- Gas/Oil Saturation Functions
--
SGOF
--
-- Gas/Oil Saturation Functions
--
          0          0          1          0
        0.1          0          0.81        0
0.2    6.77e-006          0.64        0

```

0.3	0.000216769	0.49	0
0.4	0.001646091	0.36	0
0.5	0.006936612	0.25	0
0.6	0.02116886	0.16	0
0.7	0.052674897	0.09	0
0.8	0.11385121	0.04	0
0.9	0.22197158	0.01	0
1	1	0	0

/

SOLUTION

```

--
-- -----
-- Office INIT (INIT) Data Section Version 2010.2 Oct 15 2010
-- -----
--
-- File: BASECASE_GEOMECH_TEST_INIT.INC
-- Created on: 24-Mar-2013 at: 17:51:59
--
--
*****
*****
-- *                               WARNING
*
-- *           THIS FILE HAS BEEN AUTOMATICALLY GENERATED.
*
-- *           ANY ATTEMPT TO EDIT MANUALLY MAY RESULT IN INVALID
DATA.          *
--
*****
*****
-- OFFICE-INIT-HEADER-DATA
--
--
-- -----
-- Office INIT Keywords
-- -----
--
ECHO
--
-- Equilibration Data Specification
--
EQUIL
--
-- Equilibration Data Specification
--

```

```

5150      1800      5250      1*      1*      1*      1*      1*
1*      1*      1*
--
-- 4478      1800      4550      1*      1*      1*      1*      1*
1*      1*      1*
/

```

```

ECHO
RPTRST

```

```

--
-- Restart File Output Control
--
'BASIC=5' 'FIP' 'FREQ=1' 'PRES' 'RPORV' 'RESTART' 'JV' 'MLSC'
'PORV_MOD'
'PRESMIN' 'PSAT' 'SGAS' 'SOIL' 'SWAT' 'VMF' 'XMF' 'YMF' 'ZMF' /
GMPSTBC
--
-- Principal stress boundary conditions coupled stress and fluid
flow
--
'X+' 2000 0 0 0 0 0 0 0 0 1* 1* 1* 1* 1* 1* /
'X-' 2000 0 0 0 0 0 0 0 0 1* 1* 1* 1* 1* 1* /
'Y+' 0 2000 0 0 0 0 0 0 0 1* 1* 1* 1* 1* 1* /
'Y-' 0 2000 0 0 0 0 0 0 0 1* 1* 1* 1* 1* 1* /

```

```

--side    P1X    P1Y    P1Z    P2X    P2Y    P2Z    P3X    P3Y
P3Z
--'X-'   -2000    0      0      0      -2500   200    9*/
--'X+'   -2000    0      0      0      -2500   200    9*/
--'Y-'   -2000    0      0      0      -2500   200    9*/
--'Y+'   -2000    0      0      0      -2500   200    9*/
--'Z-'   -2000    0      0      0      -2500   200    9*/
--'Z+'   -2000    0      0      0      -2500   200    9*/
/

```

```

-- set a 3000 psi total compressive traction on the X+, X-
, Y+ and Y- boundaries
-- set a 3000 psi overburden pressure (compressive stress is -ve)
-- note that the 'Z-' direction is positive downwards
GMTRABC
-- side type total
-- traction
--'X+' 1 -4300 /
--'X-' 1 -4300 /
--'Y+' 1 -4300 /
--'Y-' 1 -4300 /
'Z-' 1 -4000 /
/

```

```

SUMMARY

```

```

--
-----
-----
-- Office Summary (SUM) Data Section Version 2010.2 Oct 15 2010
-----
-----
--

```

```

-- File: BASECASE_GEOMECH_TEST_SUM.INC
-- Created on: Mar-24-2013 at: 15:30:20
--
--
*****
*****
-- *                               WARNING
*
-- *                               THIS FILE HAS BEEN AUTOMATICALLY GENERATED.
*
-- *                               ANY ATTEMPT TO EDIT MANUALLY MAY RESULT IN INVALID
DATA.                               *
--
*****
*****
--
--BPSAT
--51 51 20 /
/
FGPP
FGPT
FOPP
FOPT
FPR
--
-----
-----
-- End of Office Summary (SUM) Data Section
-----
-----
--

SCHEDULE

ECHO

GMPSTBC
--'X+' -2300 0 0 0 0 0 0 0 0 0 1 0 1 0 1 0 /
--'X-' -2300 0 0 0 0 0 0 0 0 0 1 0 1 0 1 0 /
--'Y+' 0 -2300 0 0 0 0 0 0 0 0 1 0 1 0 1 0 /
--'Y-' 0 -2300 0 0 0 0 0 0 0 0 1 0 1 0 1 0 /
--'Z+' 0 0 -2300 0 0 0 0 0 0 0 1 0 1 0 1 0 /
--'Z-' 0 0 -2300 0 0 0 0 0 0 0 1 0 1 0 1 0 /

--'X+' 0 0 0 0 0 0 0 0 0 0 1 0 1 0 1 0 /
--'X-' 0 0 0 0 0 0 0 0 0 0 1 0 1 0 1 0 /
--'Y+' 0 0 0 0 0 0 0 0 0 0 1 0 1 0 1 0 /
--'Y-' 0 0 0 0 0 0 0 0 0 0 1 0 1 0 1 0 /
--'Z+' 0 0 0 0 0 0 0 0 0 0 1 0 1 0 1 0 /
--'Z-' 0 0 0 0 0 0 0 0 0 0 1 0 1 0 1 0 /
/

WELSPECS

```


'P-01' 1* 13 13 1* 'OIL' 10 'STD' 'SHUT' 'YES' 1* 'SEG' 3* 'STD' /
/

COMPDAT

'P-01' 13 13 1 1 'OPEN' 2* 0.2 3* 'Z' 1* /
/

WELLPROD

'P-01' 'OIL' 200 3* 100 6* /
/

RPTRST

'PRES' 'RESTART' 'AIM=2' 'EFFSTRES' 'POIL' 'PRSTRESS' 'ROCKDISP'
'SOIL'
'COHESION' 'GENPLSTN' 'GENPSTRS' 'PLASDISP' 'TOTSTRES' 'DTOTSTRS' /

RPTSCHED

'PRES' 'EFFSTRES' 'TOTSTRES' 'DTOTSTRS' 'PRSTRESS' 'GMPSTBC'
'STRESBC' 'PRSTRESS' /

NSTACK

50 1* /

TUNING

10* /
14* /
2* 50 7* /

TSTEP

0.1 /

TSTEP

0.1 /

TSTEP

0.1 /

TSTEP

0.1 /

TSTEP

0.1 /

TSTEP

0.1 /

TSTEP

0.1 /

TSTEP

0.1 /

TSTEP

0.1 /

TSTEP

0.1 /

TSTEP
0.1 /

TSTEP
0.1 /

TSTEP
0.1 /

TSTEP
0.1 /

TSTEP
0.1 /

TSTEP
0.1 /

TSTEP
0.1 /

TSTEP
0.1 /

TSTEP
0.1 /

TSTEP
0.1 /

TSTEP
0.1 /

TSTEP
0.1 /

TSTEP
0.1 /

TSTEP
0.1 /

TSTEP
0.1 /

TSTEP
0.1 /

TSTEP
0.1 /

TSTEP
0.1 /

TSTEP
0.1 /

TSTEP
0.1 /

TSTEP
0.1 /

TSTEP
0.1 /

TSTEP
0.1 /

TSTEP
0.1 /

TSTEP
0.1 /

TSTEP
0.1 /

TSTEP
0.1 /

TSTEP
0.1 /

TSTEP
0.1 /

TSTEP
0.1 /

TSTEP
0.1 /

TSTEP
0.1 /

TSTEP
0.1 /

TSTEP
0.1 /

TSTEP
0.1 /

TSTEP
0.1 /

TSTEP
0.1 /

TSTEP
0.1 /

TSTEP
0.1 /

TSTEP
0.1 /

TSTEP
0.1 /

TSTEP
0.1 /

TSTEP
0.1 /

TSTEP
0.1 /

TSTEP
0.1 /

TSTEP
0.1 /

TSTEP
0.1 /

TSTEP
0.1 /

TSTEP
0.1 /

TSTEP
0.1 /

TSTEP
0.1 /

TSTEP
0.1 /

TSTEP
0.1 /

TSTEP
0.1 /

TSTEP
0.1 /

TSTEP

0.1 /

TSTEP

0.1 /

TSTEP

0.1 /

TSTEP

0.1 /

TSTEP

0.1 /

TSTEP

0.1 /

TSTEP

0.1 /

TSTEP

0.1 /

TSTEP

0.1 /

TSTEP

0.1 /

TSTEP

0.1 /

TSTEP

0.1 /

TSTEP

0.1 /

TSTEP

0.1 /

TSTEP

0.1 /

TSTEP

0.1 /

TSTEP

0.1 /

TSTEP

0.1 /

TSTEP

0.1 /

TSTEP

0.1 /

TSTEP

0.1 /

TSTEP

0.1 /

TSTEP

0.1 /

TSTEP

0.1 /

TSTEP

0.1 /

TSTEP

7 /

TSTEP

7 /

TSTEP

7 /

TSTEP

7 /

TSTEP

7 /

TSTEP

7 /

TSTEP

7 /

TSTEP

7 /

TSTEP

7 /

TSTEP

7 /

END

Information to support ECLIPSE

Sample Report of core samples test from onshore well Thailand

TRIAxIAL COMPRESSIVE STRENGTH DATA FROM WELL LKU-B13 (YOM / PRATU TAO)

Depth (m True Vertical Subsea)	Compressive Strength (psi)	Confining Pressure (psi)	Young's Modulus (psi)	Poisson's Ratio	Temperature (DEG F)
1,115 (Lower Yom)	2,485 *	500	1.83E05	0.26	Ambient
1,115 (Lower Yom)	3,200 *	1,000	1.39E05	0.16	Ambient
1,115 (Lower Yom)	4,890 *	1,500	2.78E05	0.16	Ambient
1,115 (Lower Yom)	6,618 *	2,409	1.38E05	0.07	150
1,295 (Upper Pratu Tao)	7,980 #	3,159	2.25E05	0.16	150

* determined at maximum stress # determined at yield point

SUMMARY OF ULTRASONIC VELOCITY FROM WELL LKU-B13 (YOM/PRATU TAO)

Depth (m True Vertical Subsea)		Compressional		Shear		Temperature (DEG F)
		ft/sec	μs/ft	ft/sec	μs/ft	
1,115 (Lower Yom)	Dry	9482	105.46	6022	166.05	73
1,115 (Lower Yom)	Saturated	11672	85.67	6471	154.53	150
1,295 (Upper Pratu Tao)	Dry	10708	93.39	7411	134.94	73
1,295 (Upper Pratu Tao)	Saturated	13035	76.72	6319	158.26	150

SUMMARY OF DYNAMIC MODULI FROM WELL LKU-B13 (YOM/PRATU TAO)

Depth (mTVSS)		Net Stress (psi)	Bulk Density (g/cc)	Bulk Modulus (E+06)	Young's Modulus (E+06)	Shear Modulus (E+06)	Poisson's Ratio	Temperature (DEG F)
1,115	Dry	1230	1.99	1.116	2.263	0.974	0.162	73
1,115	Saturated	1230	2.30	2.498	3.325	1.301	0.278	150
1,295	Dry	1460	2.46	1.373	3.785	1.819	0.040	73
1,295	Saturated	1460	2.57	4.041	3.723	1.383	0.346	150

Sample report for core samples test details using in P-01 well from onshore well Thailand.

CORE PLUGS TAKEN FOR SINGLE STAGE TRIAXIAL TESTS:

Core-1

PLUG	DEPTH	Rock Type	Type of Test
1	2326.03	Sandstone	UCS
SV1	2326.08	Sandstone	UCS
2	2326.23	Sandstone	MTXL
3	2326.46	Shale	UCS
4	2326.65	Shale	UCS
5	2327.65	Shale	MTXL
6	2329.44	Shale	TXL
7	2330.73	Sandstone	UCS

Total of 8 plugs

Core-2

PLUG	DEPTH	Rock Type	Type of Test
8	2332.94	Sandstone	MTXL
9	2333.76	Shale	MTXL
10	2334.42	Shale	TXL
11	2335.45	Shale	UCS
SV2	2336.50	Shale	UCS
12	2336.55	Shale	UCS
13	2338.63	Shale	TXL
14	2339.25	Shale	MTXL
15	2340.27	Shaley sand	MTXL
16	2342.53	Shale	MTXL
17	2343.18	Sandstone	UCS
18	2343.41	Sandstone	TXL
19	2344.21	Sandstone	MTXL
20	2345.52	Shale	UCS
21	2348.24	Shale	UCS
22	2349.22	Shale	MTXL
23	2349.38	Shale	TXL
24	2349.62	Sandstone	MTXL

Total of 18 plugs

Sample of core description using in P-01 well

CORE DESCRIPTION													
LKU - E17													
THAI SHELL EXPL. & PROD. CO, LTD					DATE: 24/03/2001		CORE no: 1		Sheet: 1 of 1				
					INTERVAL: 2326.00m - 2331.05m								
					CORE BARREL		MUD						
DEPTH (m)	SECONDARY STRUCTURE	Dipential Environment	G.O ₂	Fluoresce	LITHOLOGY	Pip	GRAIN SIZE						LITHOLOGICAL DESCRIPTION
							CLAY	SILT	VERY FINE	FINE	MEDIUM	COARSE	
2326													TOP CORE 1
2327	DELTA FRONT			BRIGHT YELLOW									<p>SANDSTONE: 2326.60 - 2326.35m light - medium grey, fine to very fine grained, well sorted, subangular, well indurated w/siliceous matrix, non calcareous, fine laminated carbonaceous material, dark organic streak interbedded, trace mudclasts, floating gastropod w/calcite infilling. Moderate to good visible porosity.</p>
2328				NON-CALC									<p>CLAYSTONE: 2326.35 - 2331.05m Predominantly silty claystone, very fine grained, grey to dark greenish grey, hard, massive, grading to mottled brownish claystone, mudclasts w/calcareous infilling.</p> <p>2327.35 - 5cm of very fine grained siltstone interbedded.</p> <p>2328.60 - 15cm rich of gastropods w/calcite infilling. Trace burrow and bioturbation.</p>
2329				NON-FLUORESCENT									<p>CLAYSTONE: hard, massive, greenish grey, abundant siliceous clasts w/calcareous infilling, iron oxide stained, no visible bedding plane, trace organic materials.</p>
2330				HIGH-CALCAREOUS									<p>2327.30 - 15cm trace of burrows and bioturbation, filled w/siliceous material.</p> <p>2330.70 - 30cm of silty sands interbedded, very low visible porosity trace mud clasts.</p>
2331													BOTTOM CORE 1 2331.05m

Sample of core analysis report using in P-01 well

Table 3a: Summary of Compressive Strength Test Results – Core #1

Sample Ref. No.	Depth (m)	Test Type	Stage No.	Saturated Density (g/cm ³)	Elastic Parameter		Peak Strength	
					E (GPa)	ν	σ_3' (MPa)	$\sigma_1 - \sigma_3$ (MPa)
P1	2326.03	UCS		2.39	5.93	0.32	0	25.20
PV1	2326.08	UCS		2.32	5.35	0.28	0	32.70
P2	2326.23	MTXL	Stage 1	2.34	9.46	0.16	5	60.77
			Stage 2		13.35	0.21	13	83.46
			Stage 3		13.75	0.21	23	102.30
			Stage 4		14.67	0.24	33	144.52
P3	2326.46	UCS		2.44	3.34	0.27	0	12.00
P4	2326.65	UCS		2.42	3.79	0.31	0	9.70
P5	2327.65	MTXL	Stage 1	2.50	5.62	0.30	5	31.61
			Stage 2		9.38	0.37	13	52.45
			Stage 3		11.38	0.42	23	66.60
			Stage 4		11.77	0.40	33	98.32
P6	2329.44	TXL		2.54	1.73	0.17	33	45.74
P7	2330.73	UCS		2.65	30.68	0.23	0	166.20

VITAE

Kraisingha Meepadung was born on February 1st, 1974 at Phitsanulok Province, Thailand. He received his Bachelor of Engineering in Electrical Engineering from The Sirindhorn International Institute of Technology (SIIT), Thammasat University, in 1996. He also received his Master of Engineering in Electric Power System Management from The School of Environment, Resources and Development (SERD), Asian Institute of Technology (AIT), in 1998. He has been a graduate student in the Master's Degree Program in Petroleum Engineering of the Department of Mining and Petroleum Engineering, Chulalongkorn University since 2009.